

An interesting, detailed thesis title that will catch the reader's eye and leave them mesmerised!

Andrew Raithby Casey

A thesis submitted for the degree of
Doctor of Philosophy
of the Australian National University



Australian
National
University

Research School of Astronomy & Astrophysics

Submitted 28th February 2013

NOTES ON THE DIGITAL COPY

This document makes extensive use of the hyperlinking features of L^AT_EX. References to figures, tables, sections, chapters and the literature can be navigated from within the PDF by clicking on the reference. Internet addresses will be displayed in a browser.

Most object names are resolvable in the SIMBAD (<http://simbad.u-strasbg.fr/simbad/>) astronomical database. Click on an **object** to be taken to its SIMBAD entry.

The bibliography at the end of this thesis has been hyperlinked to the NASA Astrophysics Data Service (<http://www.adsabs.harvard.edu/>). Further information on each of the cited works is available through the link to ADS.

Several of the large catalogues used in this work have been tagged with their Virtual Observatory unique identifier (e.g. ivo://astronet.ru/cas/twomass-psc). As various data centres can have different versions and implementations of the same catalogue, this ensures any analysis is repeatable by denoting the exact catalogue *and* service that was used to obtain the data. Clicking on their identifiers will resolve the service descriptions in the directory hosted by the US Virtual Observatory (<http://ww.us-vo.org>).

This page can be easily removed from the print copy...

To my cat, Mr Smigglesworth...

Disclaimer

I hereby declare that the work in this thesis is that of the candidate alone, except where indicated below or in the text of the thesis. The work was undertaken between February 2010 and July 2013 at the Australian National University, Canberra, except for the period between July 2012 and December 2012 where the work was undertaken at the Massachusetts Institute of Technology, Boston. It has not been submitted in whole or in part for any other degree at this or any other university.

A handwritten signature in black ink, appearing to read "Signature".

Andrew Raithby Casey
28th February 2013

Acknowledgments

Lorem ipsum dolor sit amet, consectetur adipiscing elit. Phasellus imperdiet volutpat turpis, vel aliquet elit tincidunt eu. Praesent convallis dolor ut tortor consectetur tincidunt. Nam ac molestie velit. Morbi luctus scelerisque purus id luctus. Fusce mattis risus eu sapien imperdiet tincidunt. Praesent laoreet blandit scelerisque. Suspendisse nec lorem velit. Nam scelerisque laoreet elementum. Sed justo urna, dapibus at varius eu, suscipit quis nibh. Integer lacinia, est sit amet accumsan luctus, nisl quam consectetur turpis, non tincidunt est ligula id sapien. Donec orci dui, convallis ac feugiat et, facilisis et velit. Donec ipsum ante, lobortis vitae auctor ac, sollicitudin a nisl. Aliquam leo leo, rhoncus ut sollicitudin et, euismod id ipsum. In in risus urna. Sed et nulla nibh, sed faucibus sem.

Maecenas est arcu, scelerisque a dapibus quis, molestie a mauris. Vestibulum egestas purus eget eros mollis placerat. Nulla porttitor, justo nec tincidunt hendrerit, nulla massa adipiscing ligula, feugiat tristique dui libero eget dolor. Phasellus id arcu id nisi faucibus eleifend vel a lacus. Vestibulum at elit eu neque vehicula elementum. Mauris bibendum massa nec urna rhoncus tempor. Curabitur in libero vitae quam vestibulum facilisis quis vitae velit. Donec tincidunt, lacus eget elementum sollicitudin, urna urna consequat ipsum, id eleifend eros augue at dolor. Praesent pellentesque, ante quis malesuada molestie, tortor lorem eleifend ante, sed rutrum massa dolor in lorem. Donec tempus, tellus eu fermentum ornare, sapien tortor tristique eros, quis blandit erat tortor eu lorem. Donec id tempus lectus. Donec ac odio eu elit molestie iaculis ac sed enim. Suspendisse et purus sem, convallis luctus mauris.

Duis massa mauris, sagittis vel dignissim non, rutrum ac nisi. Fusce ultricies mollis leo sit amet sagittis. Quisque lacinia placerat blandit. Vivamus est magna, tristique sed adipiscing in, sagittis sit amet dolor. Maecenas et nunc ipsum, in rutrum diam. Etiam ac nisl erat. Integer ac mi velit, in aliquam lacus. Etiam vitae nisi elit. Nam quam nisi, elementum eu porta eu, scelerisque vitae tortor. Nulla vel dolor magna. Aliquam suscipit, diam ac interdum pellentesque, tellus turpis sollicitudin nunc, vulputate congue massa massa vel urna. Sed a augue vel quam sollicitudin mollis.

Maecenas in lectus leo. Ut posuere lacus eget massa varius sit amet consectetur risus facilisis. Donec laoreet ornare pharetra. Maecenas vestibulum, lorem et suscipit vestibulum, enim lorem egestas eros, vitae vehicula orci sem sed dolor. Maecenas sit amet nibh nec lorem gravida hendrerit. Nulla tempus dui a lectus ornare vel viverra ipsum iaculis. Vestibulum ante ipsum primis in faucibus orci luctus et ultrices posuere cubilia Curae; Aliquam erat volutpat. In hac habitasse platea dictumst. Aenean dictum quam quis nunc tristique vitae blandit mauris dapibus. Sed velit tellus, adipiscing vitae commodo sit amet, lobortis eu orci. Morbi auctor mi eget sapien aliquet vel iaculis odio feugiat. Fusce semper risus suscipit ligula malesuada quis pretium diam rutrum. Donec varius nisi sit amet arcu interdum eu venenatis metus faucibus.

Abstract

Lorem ipsum dolor sit amet, consectetur adipiscing elit. Donec ac neque metus. Quisque a elit non justo pharetra lacinia at in dolor. Phasellus mauris mauris, sagittis id dapibus ac, facilisis vitae erat. Sed non urna mauris, nec rutrum nunc. Phasellus luctus metus nec diam hendrerit facilisis. Nulla metus ipsum, cursus in rutrum vel, rutrum ac risus. Vivamus feugiat bibendum lorem, quis iaculis nisi pellentesque at. Pellentesque fermentum tellus id lacus pharetra bibendum. Vestibulum luctus, lorem eget facilisis adipiscing, purus arcu fringilla diam, vel commodo lectus tellus non urna. Nulla elit nibh, sagittis at egestas ac, semper a elit. Nam sed dapibus sem. Mauris aliquam nulla quis arcu tincidunt auctor.

Mauris iaculis consequat porta. Quisque augue purus, auctor nec dapibus et, sodales quis nulla. Donec ipsum urna, mattis vitae consequat sed, pharetra ac dolor. Morbi placerat turpis quis eros gravida sed cursus orci posuere. Suspendisse eu malesuada arcu. Quisque turpis ante, vulputate in blandit non, molestie non leo. Quisque id erat id libero cursus pellentesque vitae a lacus. Nullam arcu ligula, sagittis id adipiscing bibendum.

Curabitur mattis consequat rutrum. Fusce vel risus non ipsum ullamcorper condimentum in a turpis. Class aptent taciti sociosqu ad litora torquent per conubia nostra, per inceptos himenaeos. Aenean sit amet odio nec augue ultricies dignissim tincidunt vel orci. Ut posuere lacinia tortor, vitae semper felis malesuada sit amet. In hac habitasse platea dictumst. Morbi vitae massa in turpis tincidunt gravida.

Cum sociis natoque penatibus et magnis dis parturient montes, nascetur ridiculus mus. Donec sodales ante eros. Suspendisse malesuada feugiat lacus vitae tincidunt. Proin eleifend arcu eget eros posuere vitae suscipit mi fringilla. Ut varius, purus id dapibus fermentum, ipsum ipsum euismod orci, vitae imperdiet nulla ligula in felis. In odio metus, ultricies sit amet sollicitudin sit amet, tempus in tortor. Nam sed turpis nulla. Fusce augue lectus, iaculis a hendrerit at, semper quis lacus. Nulla vestibulum justo nisi. Fusce egestas laoreet diam, convallis interdum elit fermentum eget. Sed ac mauris in odio dictum scelerisque.

Morbi nibh dui, adipiscing ac laoreet ac, vulputate sed metus. Sed lobortis est non lacus pellentesque a elementum tellus blandit. Ut porta, enim a ultricies mollis, arcu eros scelerisque nunc, lobortis facilisis orci ante in ipsum. Ut varius, quam eu vehicula euismod, diam leo mattis elit, ut vestibulum massa arcu a nunc. Suspendisse eleifend quam ac orci tincidunt congue. Praesent sit amet luctus lectus. Etiam interdum euismod sapien, dictum commodo nunc dictum vitae. Etiam quis sapien a felis congue ornare. Sed vel tristique tellus. In hac habitasse platea dictumst. Morbi mollis erat vel magna blandit faucibus. Duis mollis vestibulum sapien auctor mollis. Proin diam lacus, vulputate at feugiat pulvinar, mollis nec ipsum. Fusce orci enim, sollicitudin vel congue eu, tristique in diam. Pellentesque diam tellus, varius sed faucibus in, tincidunt at quam.

Aliquam erat volutpat. Curabitur rhoncus vestibulum lacinia. Sed in sollicitudin lacus. Curabitur non sem nunc. Sed nec metus a orci fermentum suscipit eu in ipsum. Sed ac arcu sed ipsum consequat sodales. Pellentesque habitant morbi tristique senectus et netus et malesuada fames ac turpis egestas.

Contents

Notes on the digital copy	0
List of Figures	ix
List of Tables	xiii
1 Introduction	1
1.1 The first of many sections	1
1.2 Wow, another section heading!	2
2 The Kinematics & Chemistry of Halo Substructures in the Vicinity of the Virgo Over-Density	5
2.1 Introduction	5
2.2 Target Selection	7
2.3 AAT Observations with AAOmega	8
2.4 Dwarf / Giant separation	9
2.5 Radial Velocities	11
2.6 Metallicities	11
2.7 Discussion	12
2.8 Carbon Stars	22
2.9 Conclusions	23
3 Hunting the Parent of the Orphan Stream	25
3.1 Introduction	25
3.2 Introduction	25
3.3 Target Selection	26
3.4 Observations	27

3.5 Analysis & Discussion	28
3.6 Conclusions	35
4 Conclusions	37
4.1 Future prospects	38
Bibliography	39
Appendix A An image of a kitten	43
Appendix B Lots of awful mathematics	45

List of Figures

1.1	The η Chamaeleontis open cluster	2
2.1	CMD of our observed regions from SDSS DR7, overlaid with the color selection criterion used to target K-giants. Appropriate Dartmouth isochrones (Dotter et al. 2008) are shown for Sgr debris at a distance of $r_\odot = 40$ kpc (Belokurov et al. 2006)	8
2.2	The sum of the Mg I triplet EWs for observations and synthetic spectra shown against the Sloan $g - i$ color. Synthetic spectra are shown for $\log g = 2$ (∇) and $\log g = 4.5$ (Δ), and points are colored by metallicity. Our dwarf/giant separation line is shown (solid).	10
2.3	Generalised histogram of V_{CSR} for our 178 K-type giants, highlighting the substructure present. The Gaussian represents the halo contribution; it is normalised such that the integral equals the number of observed stars excluding those outside a 2.5σ excess. Significant ($> 3\sigma$) kinematic deviations from the smooth distribution are appropriately grouped and labelled.	13
2.4	Our fields and observed bounds are shown with the simulated particles from multiple N -body simulations by LJM05 and LM10. These particles are distance restricted (up to 60 kpc), and color-coded by their peri-centric passage (yellow; most recent passage, red; previous passage, blue; oldest observable passage).	19

2.5 A generalised histogram (left) of the galactocentric rest frame velocities in our sample (dotted line) compared to the velocities (solid line) from the <i>N</i> -body models of LJM05, LM10 of particles within the same spatial coverage and distance range (up to $r_\odot \sim 60$ kpc) of our observed sample. Heliocentric distances for particles used to generate each velocity histogram are shown on the right. Particles are marked by their peri-centric passage. A plus (+) denotes debris from the current peri-centric passage by Sgr, circles (\circ) mark the previous passage, and squares (\square) represent debris from two previous passages. The prolate model from LJM05 is not considered in this plot (see text).	20
2.6 Metallicity histograms for K-giant members in our negative galactocentric velocity sample, which is largely populated by Sgr debris from the Northern leading arm.	21
2.7 Sloan $u - g$ and $g - r$ colors for our carbon stars, and the identified carbon stars and classifications by Downes et al. (2004). Carbon stars identified in this work have been shaded for clarity.	23
3.1 Galactocentric rest frame velocities for stars in both our observed fields (grey), and predicted Besançon velocities which have been scaled to match our observed sample size. The expected kinematic signature from ? for the Orphan Stream is highlighted, as is our kinematic selection window (green).	28
3.2 SDSS $g - r$ against the measured equivalent width of the Mg I transition at 8807 Å. Dwarf contaminants occupy the more populous upper branch. Our separation line between dwarfs and giants is shown in green.	30
3.3 Metallicities from the Ca II triplet lines versus those found from fitting isochrones to the 20 stars that meet our kinematic and surface gravity criteria. Both abundance determinations imply these stars are RGB members of the Orphan Stream at a distance of ~ 21.4 kpc (?). Consistency between these methods indicates highly likely stream membership (shaded region). The minimum isochrone [Fe/H], and a representative uncertainty of 0.2 dex for abundance measurements is shown.	31
3.4 Color magnitude diagram showing our observed candidates (grey). Observations fulfilling kinematic and gravity cuts are colored by their metallicity, and those with upper limits for surface gravity are marked as triangles (∇). Highly probable stream members (see text) are circled. Relevant 10 Gyr ? isochrones at [Fe/H] = -1.5 (dotted), -2.0 (dashed) at 21.4 kpc (?) are shown, as well as our best-fitting 10 Gyr isochrone of [Fe/H] = -1.63 at 22.5 kpc (solid).	32
3.5 Galactocentric velocities and adopted metallicities for the highest likely Orphan Stream members (black \bullet), and those with probabilities assigned as “Medium” (grey \circ ; see text).	34
3.6 Observed metallicity distribution function for the Orphan Stream candidates identified here, with comparisons to the distribution found by ? from BHB stars.	35

A.1 The aforementioned kitten	43
B.1 Orbital motion in the epicyclic approximation	47

List of Tables

1.1	Census of the η Chamaeleontis cluster prior to this work	3
3.1	Identified Orphan Stream Candidates	33

CHAPTER 1

Introduction

The labour of the astronomer in the present state of his art is much like that of one who should examine, grain by grain, the sands of the sea in the certainty that among them numerous grains must exist of extraordinary value...

– Sir John Herschel¹

1.1. The first of many sections

Lorem ipsum dolor sit amet, consectetur adipiscing elit. Duis posuere tellus eu quam pellentesque ut varius purus egestas. Nam hendrerit malesuada sapien, non molestie risus cursus at. Pellentesque habitant morbi tristique senectus et netus et malesuada fames ac turpis egestas. Sed dignissim sodales sem sed volutpat. Ut laoreet, ante sed dictum vestibulum, lacus sapien semper dui, nec rutrum velit justo eu enim. Fusce vehicula blandit ipsum, ac volutpat libero vestibulum in. Sed quis lacus mauris. Quisque congue elit in nisi lacinia ac condimentum eros pellentesque. Quisque et nisl odio, vitae eleifend neque. Oh look, a sneaky citation to my paper (? , of which I am a co-author).

Phasellus erat libero, lobortis vitae iaculis nec, congue et tortor. Donec tempus leo et nisl tincidunt porta. Nulla velit sapien, sollicitudin sit amet accumsan a, facilisis a est. Phasellus scelerisque convallis sapien, nec viverra dui tincidunt a. Nulla ligula velit, laoreet fringilla condimentum sed, euismod a est. Fusce leo sapien, rhoncus a ultricies nec, porttitor ut lectus. Sed vestibulum turpis risus, nec vestibulum diam. Morbi quis quam quis enim cursus aliquam scelerisque quis tellus. Pellentesque accumsan lectus cursus massa ultrices placerat. Nulla facilisi. Praesent fermentum erat in augue sagittis condimentum. Nullam posuere blandit urna a mollis. Cras malesuada lectus a turpis sollicitudin volutpat. Morbi semper, nisl vel mattis vehicula, sapien sapien adipiscing tortor, in accumsan tortor dolor non neque. Maecenas varius, nunc ut euismod volutpat, mauris ante faucibus magna.

¹*Memoirs of the Royal Astronomical Society*. 1826, Vol. 2, p472

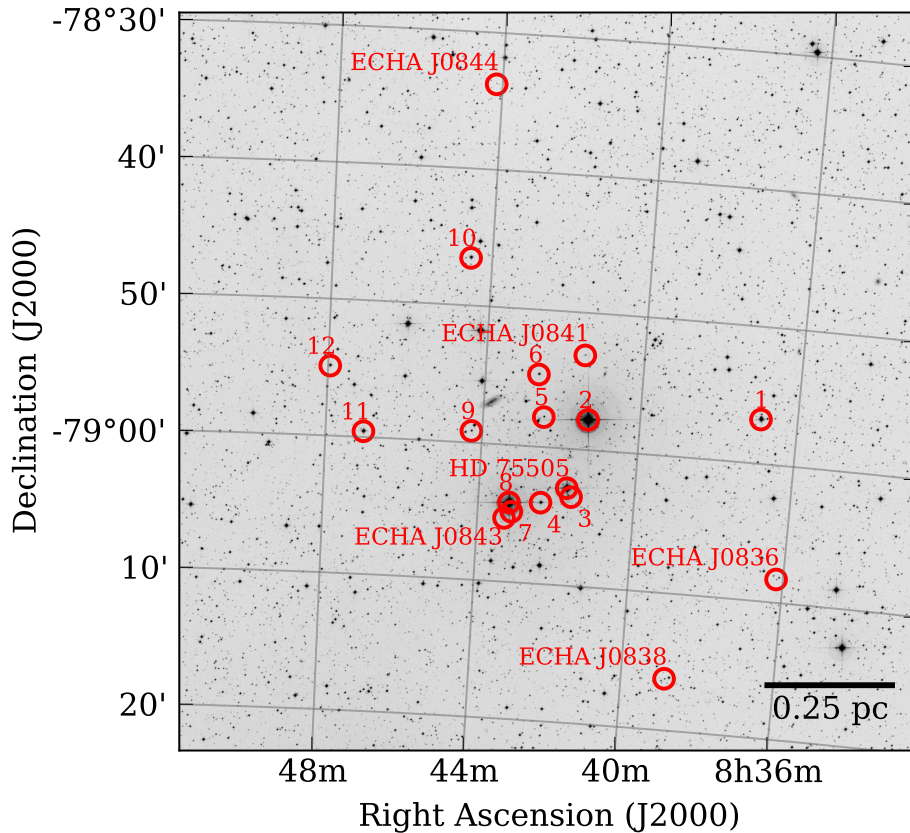


Figure 1.1 0.9×0.9 deg DSS2-IR image showing the 18 member systems of the η Cha cluster. The bright star at the centre of the image is the eponymous η Cha. The bar shows the linear scale at the 94.3 pc cluster distance.

1.1.1. A subsection

Vestibulum sed orci nec diam euismod vehicula vitae et mauris. Phasellus sagittis justo quis mauris adipiscing auctor. Suspendisse nibh erat, cursus vitae aliquam in, rutrum sed est. Nunc mollis quam quis velit vehicula fringilla. Quisque convallis, neque ut faucibus luctus, nisl ante porttitor ante, at venenatis lectus nulla sed augue. Quisque lacinia semper lacus, nec ultricies justo auctor vel. Aenean viverra aliquam est ac porttitor.

1.2. Wow, another section heading!

Sed tempor imperdiet rhoncus. Cras mi neque, pellentesque ac ultricies vitae, feugiat ut ante. Suspendisse vestibulum venenatis odio, quis pharetra mauris dapibus in. Pellentesque sagittis laoreet mi sed vestibulum. Ut iaculis venenatis urna eu tincidunt. Duis consequat est ut velit rutrum vitae placerat dolor eleifend. Nullam eget nulla massa, non accumsan libero. Sed auctor velit bibendum nisl tincidunt aliquam. Aenean pellentesque eros a lectus imperdiet rhoncus. Another citation to one of my papers (?).

Nunc non odio leo. Phasellus sodales pretium nunc suscipit bibendum. Nullam lorem turpis, varius sed bibendum id, interdum sed lectus. Ut rutrum, orci in adipiscing accumsan, velit massa dapibus metus, id volutpat nulla eros eget lorem. Ut massa massa, ornare vitae elementum ut, consequat a justo. Vestibulum tempus fermentum commodo. In vel auctor nisi. Mauris id turpis nisi. Nulla eget magna eu magna rhoncus pulvinar. Morbi enim

ligula, feugiat et rutrum in, posuere eget lacus. Suspendisse adipiscing, erat in hendrerit dictum, est tellus vestibulum justo, et sodales mi dolor sed purus.

In porttitor purus et metus adipiscing molestie. Curabitur scelerisque, sem ac sodales sodales, neque metus commodo massa, eu pulvinar ante lectus eu orci. Mauris non odio vel enim scelerisque porttitor ac ac lacus. Pellentesque habitant morbi tristique senectus et netus et malesuada fames ac turpis egestas. Phasellus id dolor dui. Cras non neque vel turpis posuere commodo et nec leo. Nulla dictum rutrum nisi ac rhoncus. Aenean lobortis tempor magna viverra iaculis. Ut sit amet nunc mi. Integer iaculis condimentum diam non dignissim. Duis bibendum auctor velit id scelerisque.

Nulla tincidunt tortor ac odio posuere eget semper mauris tristique. Vestibulum congue magna sed arcu tincidunt id pharetra nisi hendrerit. Duis erat nulla, fringilla sed tempus at, sodales a libero. Nunc ullamcorper dapibus dui, ut varius tellus ullamcorper quis. Pellentesque odio lacus, molestie quis porta vitae, ornare eget massa. Integer hendrerit sapien ac massa lobortis in malesuada quam dignissim. Aliquam feugiat, nisl ut semper auctor, purus nunc iaculis ipsum, non tristique nibh felis a ipsum. Pellentesque odio lacus, molestie quis porta vitae, ornare eget massa. Ut sit amet nunc mi. Integer iaculis condimentum diam non dignissim. Duis bibendum auctor velit id scelerisque.

You can click on objects and be taken to their SIMBAD entry, like this: [Large Magellanic Cloud](#). All of the objects in Table 1.1 are resolvable in SIMBAD.

Table 1.1 Census of the [\$\eta\$ Chamaeleontis cluster](#) prior to this work

Name	Right Ascension [J2000 deg]	Declination [J2000 deg]	Spectral Type [†]	V [‡] [mag]	Binary?*
ECHA J0836.2–7908	08 36 10.6	−79 08 18	M5.3	17.66	suspected
RECX 1	08 36 56.2	−78 56 46	K7.0	10.61	yes
ECHA J0838.9–7916	08 38 51.5	−79 16 14	M5.0	16.82	suspected
η Cha (RECX 2)	08 41 19.5	−78 57 48	B8V	5.46	suspected
ECHA J0841.5–7853	08 41 30.6	−78 53 07	M4.7	17.07	
RECX 3	08 41 37.2	−79 03 31	M3.0	14.35	
HD 75505	08 41 44.7	−79 02 53	A6	7.27	
RECX 4	08 42 23.7	−79 04 04	M1.3	12.79	
RECX 5	08 42 27.3	−78 57 49	M3.8	15.20	
RECX 6	08 42 39.0	−78 54 44	M3.0	14.08	
RECX 7	08 43 07.7	−79 04 52	K6.9	10.84	yes
RS Cha (RECX 8)	08 43 12.2	−79 04 12	A8V+A8V	6.28	triple?
ECHA J0843.3–7905	08 43 18.4	−79 05 21	M3.4	13.97	
ECHA J0844.2–7833	08 44 09.1	−78 33 46	M5.5		suspected
RECX 9	08 44 16.6	−78 59 09	M4.4	15.00	yes
RECX 10	08 44 32.2	−78 46 32	M0.3	12.53	
RECX11	08 47 01.8	−78 59 35	K6.5	11.13	
RECX 12	08 47 56.9	−78 54 54	M3.2	13.17	suspected

[†]? (K and M members), ? (early-type members)

[‡]Photometry from ?

* ECHA J0844.2 has an elevated position in the cluster CMD

CHAPTER 2

The Kinematics & Chemistry of Halo Substructures in the Vicinity of the Virgo Over-Density

Parts of this chapter have been previously published as '[Kinematics & Chemistry of Halo Substructures: The Vicinity of the Virgo Over-Density](#)', Casey, A. R., Keller, S. C., Da Costa, G., 2012, AJ, 143, 88C. The work is presented here in expanded and updated form.

2.1. Introduction

The proportion of substructure recently uncovered in the Galaxy has highlighted the crucial involvement accretion has played in the formation of the Milky Way (see [Helmi 2008](#), and references therein). Properties of these stellar structures allow us to probe the formation mechanisms and history of the Galaxy. Recent studies ([Carollo et al. 2007, 2010](#)) have suggested multiple evolutionary paths are required for galaxy formation to reconcile observational evidence, although this is a subject of ongoing debate ([Schönrich et al. 2011](#)). Regardless, the dissipation-less merging paradigm is widely accepted and consistent with favoured Cold Dark Matter (Λ CDM) cosmology models. Through the examination of ongoing accretion events in the Milky Way and fossils from previous mergers we can trace the evolution of the outer most regions of the Galaxy (e.g., [Helmi & White 2001](#)).

Accretion is at least partly (e.g., [Starkenburg et al. 2009](#)), if not entirely responsible for the formation of the stellar halo. [Bell et al. \(2008\)](#) compared Sloan Digital Sky Survey ([York et al. 2000](#), hereafter SDSS) data to galaxy formation simulations using different dark halos and found that observations are consistent with the stellar halo being entirely formed by hierarchical merging of accreted satellites (see also [Xue et al. \(2011\)](#)).

Unquestionably the most prominent ongoing accretion event within the Milky Way is that of the Sagittarius (Sgr) dwarf Spheroidal (dSph) galaxy. Originally discovered by [Ibata et al. \(1994\)](#) as a co-moving group of K- and M-type giants, the tidal tails of Sgr circle our Galaxy. As such they have been extensively traced with red-clump stars ([Majewski et al. 1999](#)), carbon stars ([Totten & Irwin 1998; Ibata et al. 2001](#)), RR Lyrae stars ([Ivezic et al.](#)

2000; Vivas et al. 2005; Keller et al. 2008; Watkins et al. 2009; Prior et al. 2009a), A-type stars (Newberg et al. 2003), BHB stars (Ruhland et al. 2011) and K/M-giants (Majewski et al. 2003; Yanny et al. 2009; Keller et al. 2010). Tracers originating from the host system can be unequivocally identified with spatial and kinematical information because they remain dynamically cold, and are identifiable as kinematic substructures long after they are stripped from their progenitor (for example Ibata & Lewis 1998; Helmi & White 1999).

Stellar tracers within these tidal tails are kinematically sensitive to the galactic potential. This has led various groups to model the Sgr interaction with different dark matter profiles. Martínez-Delgado et al. (2004) traced the Northern leading arm and found a near spherical or oblate ($q \approx 0.85$) dark matter halo best represented the observed debris, coinciding with the findings of Ibata et al. (2001). In contrast, Helmi (2004) found evidence in the Sgr leading debris that most favoured a prolate ($q = 1.25$) halo. Vivas et al. (2005) found that either a prolate or spherical model of Helmi (2004) would fit their RR Lyrae observations, rather than those of an oblate model. Johnston et al. (2005) later pointed out that no prolate model can reproduce the orbital pole precession of the Sgr debris but an oblate potential could. Law et al. (2005, hereafter LJM05) performed simulations using data of the Sgr debris from the 2-Micron All Sky Survey (2MASS) catalogue and found that the kinematics of leading debris was best fit by prolate halos, whereas the trailing debris typically favoured oblate halos. Prior et al. (2009b) reached a similar conclusion.

Belokurov et al. (2006) found an apparent bifurcation within the Sgr debris which Fellhauer et al. (2006) argued can only result from a dark halo having a near spherical shape. Law et al. (2009) introduced a tri-axial model with a varying flattening profile q , which replicates the orbital precession seen and matches kinematic observations of the Sgr debris. However Law & Majewski (2010) (hereafter LM10) concede this may be a purely numerical solution as tri-axial halos are dynamically unstable. They emphasize that more kinematic measurements in other regions of the Sgr stream are required.

After the Sgr stellar stream, the Virgo Over-Density (VOD) is arguably the next most significant substructure within our Galaxy. The first over-density in the vicinity of the VOD was observed as a group of RR Lyrae stars by the QUEST survey (Vivas et al. 2001). The collaboration later named this the “12^h.4 clump” (Zinn et al. 2004). The broad nature of the VOD was later uncovered from the SDSS catalogue as a diffuse over-density of main-sequence turnoff stars centered at $r_\odot \sim 18$ kpc (which Newberg et al. 2002, dubbed as S297+63-20.5). The nomenclature on the substructure names within this region is varied, however in this paper when referring to the VOD we are discussing the spatial over-density of stars within the region, separate from any detected co-moving groups.

The difficulty arises in accurately distinguishing the VOD as there are multiple substructures along this line-of-sight. Duffau et al. (2006) took observations of BHB and RR Lyrae within the “12^h.4 clump” and found a common velocity of $V_{GSR} = 99.8$ km s⁻¹ with $\sigma_v = 17.3$ km s⁻¹. It should be noted that the dispersion in kinematics measured by Duffau et al. (2006) is essentially their velocity precision, so the substructure may possess a much smaller kinematic dispersion. This co-moving group was coined the Virgo Stellar Stream (VSS) to differentiate it from the broad spatial over-density. This distinction from the VOD was somewhat strengthened with new distance measurements which placed the VOD centroid at $r_\odot = 16$ kpc (Jurić et al. 2008; Keller 2010), and the VSS 3 kpc further away (Duffau et al.

2006). Although, when considered in the light of systematic and observational uncertainties, this is of marginal significance. Additionally, Jurić et al. (2008) suggests the VOD may extend between $r_\odot = 6$ to 20 kpc, which further complicates the matter of distance separation.

The relationship between the VSS and the S297+63-20.5 over-density is still unclear. Newberg et al. (2007) found a kinematic signature at $V_{GSR} = 130 \pm 10 \text{ km s}^{-1}$ for members of the VOD/S297+63-20.5, which is extremely close to the VSS peak. The VSS and S297+63-20.5 are co-incident in space, but their velocity difference has not yet been reconciled. The distance measurements between S297+63-20.5 and the VSS are similar enough (~ 1 kpc) within probable distance uncertainties for Newberg et al. (2007) and Prior et al. (2009b) to infer they are part of the same structure. Newberg et al. (2007) estimate a distance to S297+63-20.5 of $r_\odot = 18$ kpc from $g_0 = 20.5$ turnoff stars, but they concede the structure is likely dispersed along the line-of-sight as the Color-Magnitude Diagram (CMD) for this region does not demonstrate a tight sequence. Certainly this region of sky, aptly coined the ‘Field of Streams’ by Belokurov et al. (2006), is complex territory.

Photometric studies are inadequate to fully untangle this region. Kinematics are essential to identify co-moving groups that are distinct from the general halo field. Chemical information is vital to accurately distinguish these substructures and understand their origins. However, very few studies have directly investigated metallicities for these stars. In this paper we present spectroscopic observations of K-giants in this region. Sgr stream kinematics are used to probe the shape of the dark matter halo in the Galaxy. We report both the velocities and metallicities of these giants in an effort to help untangle this accretion-dominated region.

Target selection methodology is outlined in the next section which is followed with details regarding the observations. Techniques used to separate K-giants from dwarfs are discussed in §2.4, and our analysis procedure for kinematics (§2.5) and metallicities (§2.6) follows. A discussion of substructures is outlined in §2.7, and in §2.8 we report the carbon stars discovered in our sample. In §2.9 we conclude with some final remarks and critical interpretations.

2.2. Target Selection

When the presence of a stellar substructure is uncovered, K-giants provide excellent candidates for spectroscopic follow-up. They allow for precise radial velocities and chemical abundances. In order to specifically target K-giants we have chosen candidates within the color selection box shown in Figure 2.1, taken from the SDSS DR7 catalogue. This selection box favors a metal-poor population at Sgr stream-like distances (~ 40 kpc) but will also contain similarly metal-poor stars at VOD/VSS distances (~ 20 kpc) without being significantly biased. Field dwarfs are expected to contaminate the sample due to their similarity in colors. Although K-dwarfs are difficult to distinguish photometrically we can spectroscopically separate these through the equivalent width (EW) of the gravity-sensitive Mg I triplet lines at 5167.3, 5172.7, and 5183.6 Å (see §2.4).

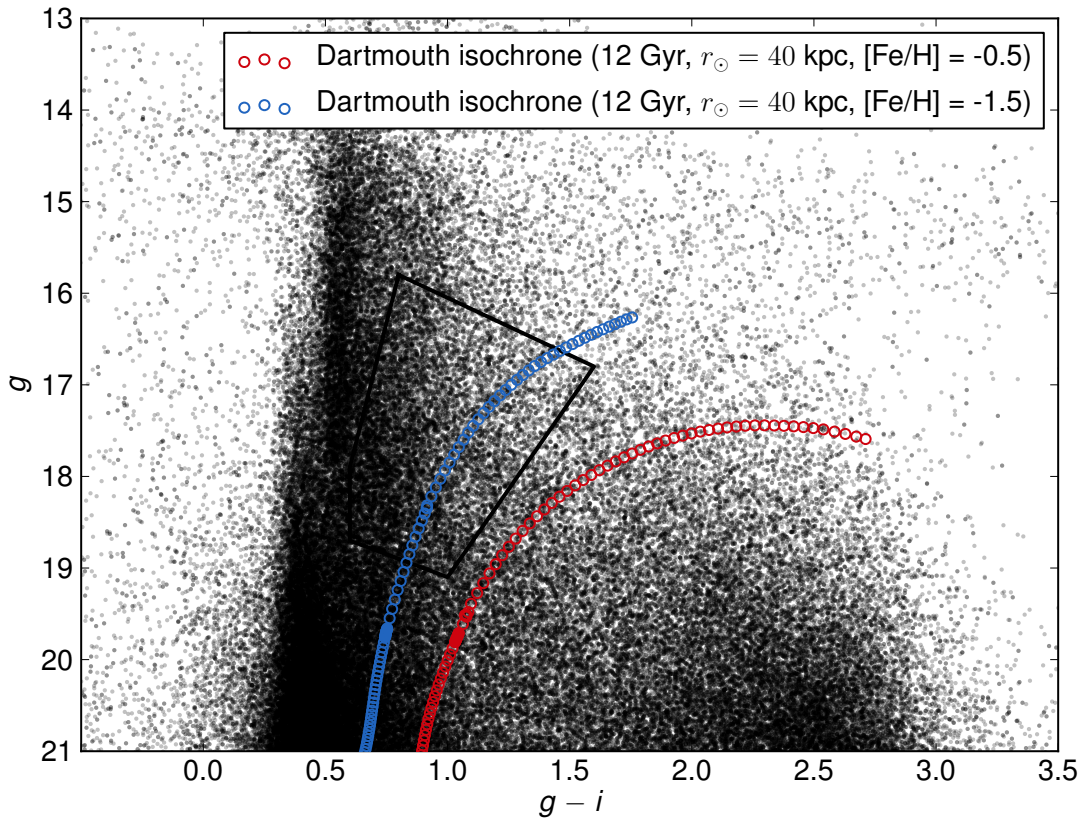


Figure 2.1 CMD of our observed regions from SDSS DR7, overlaid with the color selection criterion used to target K-giants. Appropriate Dartmouth isochrones (Dotter et al. 2008) are shown for Sgr debris at a distance of $r_{\odot} = 40$ kpc (Belokurov et al. 2006)

2.3. AAT Observations with AAOmega

Our targets were observed over two runs using AAOmega on the 3.9-m Anglo-Australian Telescope at Siding Springs Observatory in New South Wales, Australia. AAOmega is a double-beam, multi-object (392) fibre-fed spectrograph covering a two degree field of view. The targets were observed in normal visitor mode in April 2009. Throughout all observations, sufficient sky fibres (~ 30) were allocated to ensure optimal sky subtraction. In total 3,453 science targets were observed across 4 fields within the VOD/Sgr region, as outlined in Table ???. Multiple configurations were observed for most fields to permit measurements of bright ($i < 16$) and faint ($i > 16$) stars, as well as repeat observations on a subset of stars.

The beam was split into the red and blue arms using the 5700 Å dichroic. The 580V grating in the blue arm yields spectra between 370-580 nm, with a resolution of $R = 1300$. In the red arm we used the 1000I grating ($R = 4400$) which spans the spectral range from 800-950 nm. This coverage includes the Ca II NIR Triplet (CaT), which is used for radial velocities and metallicities. Science targets on each configuration were limited to 1.5 magnitudes in range to minimise scattered-light cross talk between fibres. Globular clusters NGC 5024, 5053 and 5904 were observed as radial velocity and metallicity standards.

The data was reduced using the 2DFDR¹ pipeline. After being flat-fielded, the fibres were throughput calibrated and the sky spectrum was subtracted using the median flux of the dedicated sky fibres. Wavelength calibration was achieved from arc lamp exposures taken between each set of science fields. Multiple object frames were combined to assist with cosmic ray removal.

2.4. Dwarf / Giant separation

When discussing our data with respect to stellar streams and substructures within the halo, we are referring only to K-type giants. Dwarfs that fall within our apparent magnitude limit are not sufficiently distant to probe halo substructures. Our resolution is adequate such that the Mg I triplet lines can be individually measured and used to discriminate against dwarfs.

A grid of synthetic spectra has been generated to quantitatively establish a suitable giant/dwarf separation criterion. The grid was generated using Castelli & Kurucz (2004) model atmospheres with MOOG² and the line list of Kurucz & Bell (1995). Spectra were also generated using stellar parameters for the Sun and Arcturus. The strength of the Mg I lines were tuned to match both the Solar and Arcturus atlases of Hinkle et al. (2003). Girardi et al. (2004) isochrones have been used to translate our de-reddened $g - i$ color range to effective temperature. Reddening is accounted for using the Schlafly & Finkbeiner (2011) corrected dust maps of Schlegel et al. (1998) assuming a Fitzpatrick (1999) dust profile where $R_V = 3.1$. The corresponding effective temperature region ranges from 3900 to 5200 K, and is stepped at 25 K intervals. We have assumed typical K-type surface gravities of $\log g = 2$ for giants and $\log g = 4.5$ for dwarfs. Metallicities of $[Fe/H] = -0.5, -1.5$, and -2.5 were considered for both surface gravities.

All synthetic spectra was mapped onto the same wavelength intervals before the flux was convolved with a Gaussian kernel of 3.03 Å to match our 580V observations. Mg I line strengths for our observations and synthetic spectra are shown against $g - i$ in Figure 2.2. As expected, there is an overlap of Mg I strengths between metal-rich “giants” ($\log g = 2$) and metal-poor “dwarfs” ($\log g = 4.5$). However we do not expect metal-poor dwarfs to be a principle contaminant due to their intrinsically low luminosities and comparative rarity.

Using our synthetic grid, we have varied the slope and offset of our separation line to assess the effectiveness in differentiating giants from dwarfs. A linear rule has been adopted to differentiate the populations and maximise giant recoverability with minimal contamination. Using the rule,

$$EW_{MgI} < 3(g - i)_o + 0.5 \quad (2.1)$$

we identify 185 giants in our observed fields. An analysis of our 185 giant candidates revealed three stars with high proper motions (PPMXL Catalog Roeser et al. 2010), all of which lay close to our dwarf/giant separation line. This suggests they are dwarfs, and they have been excluded. Some possible giant targets were also discarded due to insufficient S/N, or because the Mg I triplet fell on bad columns of the detector. All efforts were made

¹<http://www.ao.gov.au/AAO/2df/aaomega>

²<http://www.as.utexas.edu/~chris/moog.html>

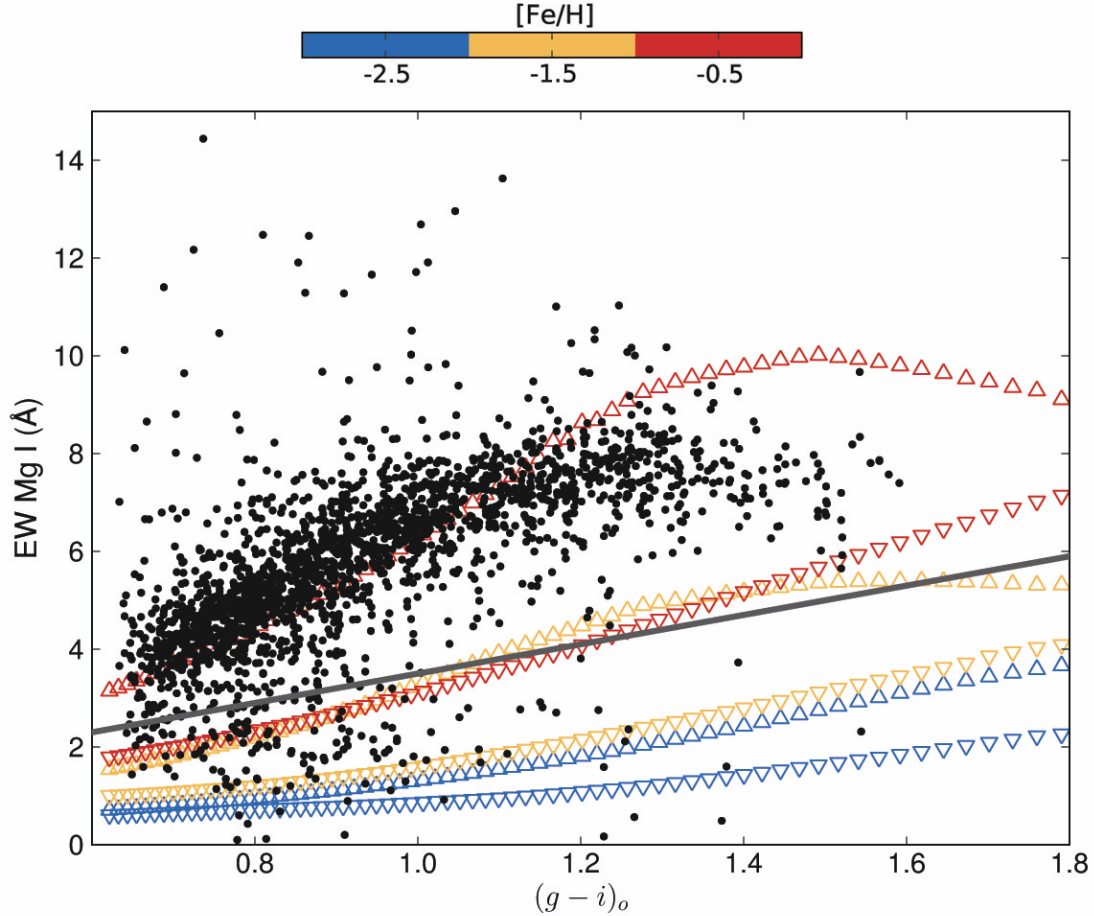


Figure 2.2 The sum of the Mg I triplet EWs for observations and synthetic spectra shown against the Sloan $g - i$ color. Synthetic spectra are shown for $\log g = 2$ (∇) and $\log g = 4.5$ (Δ), and points are colored by metallicity. Our dwarf/giant separation line is shown (solid).

to minimise these losses. The distilled giant sample size is 178 stars. All identified K-giant stars in our distilled sample had no proper motion detectable above measurement errors.

2.5. Radial Velocities

The Ca II triplet absorption lines at 8498.0, 8542.1 and 8662.1 Å have been used to measure radial velocities. These lines are strong, and easily identifiable in Red Giant Branch (RGB) stars even at low resolution. Observed spectra have been cross-correlated with a synthetic spectrum of a typical K-giant ($T_{eff} = 4500$ K, $\log g = 2$, $[Fe/H] = -1.5$) to measure radial velocities. Heliocentric corrections were also applied. Radial velocity measurements made of the standard stars in our globular clusters agree (within 3 km s⁻¹) with the catalogue of [Harris \(1996\)](#) (2011 edition). Further, a number of our targets were observed on multiple fields, which allows us to calculate the internal measurement error. The differences between multiple measurements of the same target were calculated and they form a half-normal distribution with a HWHM = 3.58 km s⁻¹.

In order to compare our kinematic results in a homogenous manner, we have translated our heliocentric velocities to a galactocentric frame. We have adopted the circular velocity of the Local Standard of Rest (LSR) at the Sun as 220 km s⁻¹ ([Kerr & Lynden-Bell 1986](#)) and accounted for the Sun's peculiar velocity to the LSR by using 16.5 km s⁻¹ towards $l = 53^\circ$, $b = 25^\circ$ ([Mihalas & Binney 1981](#)). The corrected line-of-sight velocity is then given by,

$$\begin{aligned} V_{GSR} = & V_{OBS} + 220 \sin l \cos b + 16.5 \\ & \times [\sin b \sin 25 + \cos b \cos 25 \cos(l - 53)] \end{aligned} \quad (2.2)$$

where V_{OBS} is the heliocentric-corrected observed line-of-sight velocity. A caveat to this reference transformation is that other authors in the literature have used slightly different formulae to transpose their kinematics to a galactocentric frame. This will result in possible systematic shifts in velocities between authors of up to ~ 11 km s⁻¹.

2.6. Metallicities

We have measured metallicities for our giants using the strength of the Ca triplet lines. This technique was originally empirically described for individual stars in globular clusters ([Armandroff & Da Costa 1991](#)). A spectroscopic analysis using VLT/FLAMES observations of RGB stars from composite populations led [Battaglia et al. \(2008\)](#) to conclude that a calibrated CaT-[Fe/H] relationship can be confidently used in composite stellar populations (see also [Rutledge et al. 1997; Starkenburg et al. 2010](#)). The caveat to this technique is that a luminosity (specifically $V - V_{HB}$) is required for calibration, and we have to assume a V_{HB} luminosity here. Johnson V-band magnitudes for our giants were calculated from SDSS *ugriz* photometry using [Jester et al. \(2005\)](#) transformations. The weaker third Ca triplet line is more susceptible to noise and residual sky-line contamination ([Tolstoy et al. 2001; Battaglia et al. 2008](#)). Consequently, only the strongest two CaT lines (8542 and 8662Å) have been used to form a reduced EW (W') such that,

$$\sum W = EW_{8542} + EW_{8662} \quad (2.3)$$

$$W' = \sum W + 0.64 (\pm 0.02) (V - V_{HB}) \quad (2.4)$$

and the metallicity linearly varies with W' where,

$$[\text{Fe}/\text{H}]_{\text{CaT}} = (-2.81 \pm 0.16) + (0.44 \pm 0.04)W' \quad (2.5)$$

Using this calibration our globular cluster standard stars (with known V_{HB} magnitudes) have metallicities that match well with the [Harris \(1996\)](#) catalogue (2011 edition). Only K-giants within the valid calibration range ($0 > V - V_{HB} > -3$) were considered for metallicities. We assume that we have two dominant substructures present in our observations; the leading arm of Sgr and the Virgo Over-Density (see §2.7.1). The Sgr stream dominates our negative V_{GSR} population, and our positive kinematic space primarily comprises VOD and VSS members. As such we have separated our population at $V_{GSR} = 0 \text{ km s}^{-1}$ into two samples with assumed V_{HB} magnitudes. Although this introduces a (known) systemic effect, it is a required assumption to estimate the metallicity distribution of each population.

The horizontal branch magnitude assumed for the VSS/VOD has been ascertained from previous RR Lyrae studies. As RR Lyrae stars sit on the horizontal branch, the V_{HB} is taken as the V-band median of four [Prior et al. \(2009b\)](#) and three [Duffau et al. \(2006\)](#) VSS members to yield $\langle V \rangle = 17.09$. This combined value precisely matches the mean reported by [Duffau et al. \(2006\)](#). In our K-giant sample with positive galactocentric velocities, we assume $V_{HB} = 17.09$ which implies these stars are at a distance of $\sim 20 \text{ kpc}$.

As the distance to the Sgr debris varies greatly throughout the halo, the horizontal branch magnitude varies with the position along the stream. Through CMD comparisons with the Sgr core ([Bellazzini et al. 2006](#)), [Belokurov et al. \(2006\)](#) determined distances along the two branches of the Sgr bifurcation. Revised distance measurements by [Siegel et al. \(2007\)](#) (as tabulated in Table 1 of LM10) have been crucial in constraining dark halo models. Our observations lay on the edge of Branch A (Figure ??).

We have assumed distances to these stars by interpolating their position along a cubic spline fitted to published distances ([Siegel et al. 2007](#)). Recent distance measurements of the stream by [Ruhland et al. \(2011\)](#) match the stream distances used here within the uncertainties. The horizontal branch magnitude V_{HB} is calculated using this assumed distance and the known luminosity of RR Lyrae stars ($M_V = +0.69$; [Tsujimoto et al. 1998](#)). Typical V_{HB} magnitude derived for the Sgr members is 18.7, corresponding to a distance of $\sim 41 \text{ kpc}$. Reddening is accounted for using the [Schlegel et al. \(1998\)](#) maps with [Schlafly & Finkbeiner \(2011\)](#) corrections as described in §2.4. Uncertainties in distance are not interpolated; they are taken as the largest published uncertainty of the closest neighbouring data points, and this is propagated through to our reported metallicity uncertainties. The kinematics and metallicities derived for our giant sample are discussed in the following section.

2.7. Discussion

2.7.1. Substructure Identification

A significant kinematic deviation from a canonical halo population signifies a co-moving group. There are multiple substructures along our line-of-sight. These features are identified first and discussed separately. We have represented our galactocentric velocities with a

generalised histogram (Figure 2.3) to quantitatively compare the observed stellar kinematics against the hypothesis that the parent distribution can be described by a canonical halo where $\mu = 0 \text{ km s}^{-1}$, and $\sigma = 101.6 \text{ km s}^{-1}$ (Sirko et al. 2004).

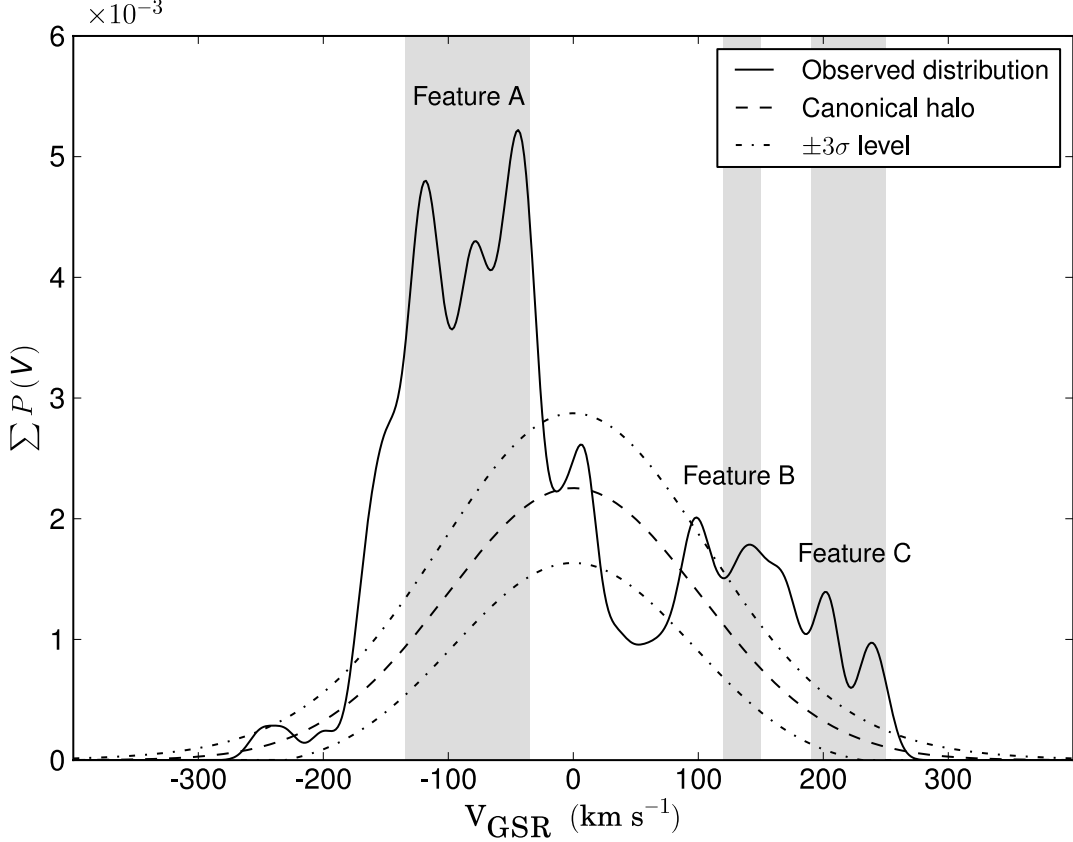


Figure 2.3 Generalised histogram of V_{GSR} for our 178 K-type giants, highlighting the substructure present. The Gaussian represents the halo contribution; it is normalised such that the integral equals the number of observed stars excluding those outside a 2.5σ excess. Significant ($> 3\sigma$) kinematic deviations from the smooth distribution are appropriately grouped and labelled.

The generalised histogram represents each data point with a Gaussian kernel of an equal deviation. As our internal kinematic errors between multiple measurements summate to a half-normal distribution with a FWHM of 7.16 km s^{-1} , we have opted for a sigma value of 10 km s^{-1} for the generalised histogram in Figure 2.3 to avoid under-smoothing. The most significant ($> 3\sigma$) kinematic peaks have been labeled Features A, B, and C. Features A and C are our most significant structures, and the importance of Feature B becomes more evident through Monte-Carlo simulations.

Velocities and metallicities of our K-giants, shown in the left panel of Figure ??, were binned into grid blocks of 15 km s^{-1} and 0.3 dex – roughly twice the error in each dimension. To interpret these data a population of 178 stars was randomly drawn from a simulated halo with canonical kinematics. Metallicities were randomly assigned using the observed halo Metallicity Distribution Function (MDF) of Ryan & Norris (1991). Each simulated population was binned identically to our observed sample. Simulation grid blocks with counts equal to or exceeding stars in the equivalent observed grid block were noted, and summed after 10,000 simulations. Results from our Monte-Carlo simulations are illustrated in Figure ?? (right). The identified Features A, B, and C in our results were consistently

significant when the grid was midpoint offset in both dimensions, except for the grid-block centered at $\sim 185 \text{ km s}^{-1}$ and ~ -1.4 dex, which has consequently been left unlabelled.

Substructure becomes statistically significant when the observed grid blocks are rarely replicated in Monte-Carlo simulations. Specifically, the number of members in Feature A was never reproduced in some grid bins. This feature is well in excess of the halo and has a wide spread in kinematics. Chou et al. (2007) mapped the Sgr debris across the sky using K/M-giants and found galactocentric velocity signatures between -205 km s^{-1} to -31 km s^{-1} in this region. As such we attribute this wide, significant kinematic peak as the leading arm of the Sgr tidal tail. Feature A is discussed in the next section. Another feature where grid blocks were never reproduced in our simulations was Feature C. This feature may also be attributed to Sgr debris and is discussed further in §2.7.4.

The clump of stars in the velocity bin centered on $V_{GSR} \approx 130 \text{ km s}^{-1}$ and $[\text{Fe}/\text{H}] \approx -2$ was replicated only $\sim 1\%$ in 10,000 simulations. We attribute these stars to the Virgo Stellar Stream, as they are coincident in spatial position, velocity, and metallicity with previously reported values of the VSS obtained by F turnoff/BHB stars (Newberg et al. 2007) and RR Lyrae stars (Prior et al. 2009b). Feature B is discussed in §2.7.3.

2.7.2. Feature A – Sagittarius Debris

Our observed fields are overlaid upon a panoramic projection of the Sgr stream and the “Field of Streams” (Belokurov et al. 2006) in Figure ???. This is a crowded region of globular clusters, substructures and overlapping stellar streams, primarily populated by the Sgr Northern leading arm. Simply from a spatial perspective, we expect the Sgr debris to dominate our data. Although the VOD is present, it is much more diffuse.

Comparing Sagittarius Debris to Dark Matter Halo Models

In order to investigate the spatial coverage and kinematics of our Sgr members we have compared our data with the constant flattening spheroidal models of LJM05, and the more recent tri-axial model of LM10. The simulated data output from these models is readily available online³, and the released models have the best-fitting parameters for each dark halo shape (prolate, spherical, oblate and tri-axial). These are the only simulations available which make use of an all-sky data set; the 2MASS M-giant sample. We have not considered particles farther than 60 kpc to match realistic observation limitations. The 10^5 model Sgr debris particles from their simulations are represented along the best-fit great-circle (Λ_\odot, B_\odot) where the longitudinal coordinate Λ_\odot is zero in the direction of the Sgr core and increases along the trailing debris. For comprehensive details of the simulations the reader is referred to the papers of Law et al. (2005) and Law & Majewski (2010).

The Northern leading arm of Sgr is particularly sensitive both kinematically and spatially to the shape of the Milky Way dark halo (Figure 2.4). The spherical, oblate and tri-axial models predict the Sgr stream to pass directly through our fields, whereas the prolate model predicts only the edge of the stream near this region and no particles directly in our fields. Spatially, the prolate model predicts the Sgr stream to pass much lower in latitude (B_\odot) than

³<http://www.astro.virginia.edu/~srm4n/Sgr/>

our observed fields. When we extend a rectangle bounded by the edges of our fields (as per the zoomed insets in Figure 2.4) a mere two model particles are found. The 10^5 model particles are proportional to the stream density so the lack of model particles implies a negligible stream concentration in our observed region. Observationally, when the number of field configurations is accounted for our observed Sgr K-giants are uniformly distributed across the fields. If this prolate halo model is a true representation of the Sgr debris, this does not exclude the potential of finding some Sgr debris in our fields. However, it does imply that if the LJM05 prolate model is an accurate representation of the dark halo then Sgr would not be the dominant population – contrary to our preferred interpretation of the observations.

In comparison, the tri-axial, spherical and oblate models predict varying amounts of debris from previous peri-centric passages in our fields. A kinematic comparison against our observations is necessary to evaluate model predictions. As the prolate model has only two simulated particles within our extended bounds there is no qualitative kinematic comparison to be made for this model, therefore the prolate model is excluded from further kinematic analysis.

The number of predicted particles observable differs between models. Consequently, the kinematics for each model have been represented as a generalised histogram (Figure 2.5). For consistency all simulation output and observed data has been convolved with a Gaussian kernel of 10 km s^{-1} ; the sigma used for the previous generalised histogram in Figure 2.3. Predicted distances and peri-centric ages are shown, demonstrating that debris from multiple passages are predicted along the line-of-sight. A much tighter velocity sequence is predicted by the tri-axial model than the constant flattening models. This is because the tri-axial model predicts a peri-center almost precisely in our observable region, whereas the spherical and oblate models predict a large wrap along the line-of-sight, resulting in a wide spread of distances and velocities.

Predicted distances are consistent with what we would expect from our observations. The median luminosities of our giants is $g \sim 17.5$, so for the tri-axial model particles at 45 kpc this corresponds to an absolute magnitude of $M_g \sim -0.8$; quite reasonable for a K-giant. Similarly for the spherical and oblate models, typical distances of $\sim 25 \text{ kpc}$ will yield luminosities of $M_g \sim +0.5$ which is also reasonable.

The spherical and oblate models also predict close-by debris with extremely negative galactocentric velocities. This signature is not represented in our data. The lowest observed velocity is $\sim -250 \text{ km s}^{-1}$ and we have only two observations less than $V_{GSR} < -200 \text{ km s}^{-1}$. In contrast, the spherical/oblate models predict velocities well below $V_{GSR} < -300 \text{ km s}^{-1}$. These predicted highly negative velocities were also not found in Sgr RR Lyrae observations taken by [Prior et al. \(2009a\)](#). If the dark matter potential is well-represented by either an oblate or spherical halo, then this discrepancy must be reconciled.

The oblate and spherical model also illustrate a similar signature at $r_\odot \sim 12 \text{ kpc}$, with particle velocities ranging between $-100 < V_{GSR} < 0 \text{ km s}^{-1}$. This is the edge of a predicted crossing-point between different wraps of the stream, which occurs at $\sim 12 \text{ kpc}$. These particles (and the positive kinematic signature around $\sim 20 \text{ kpc}$ in the oblate model), are relatively minor signatures when compared to the Northern arm feature. If these signatures are present in our observed fields, their relatively low density compared to the Northern arm feature

would prevent them from appearing as significant.

Although the predicted velocity distribution is narrower than what we observe, the LM10 tri-axial dark halo model best fits our observations. The observed sample broadens most prominently towards more negative galactocentric velocities at $\sim -200 \text{ km s}^{-1}$, considerably higher than oblate/spherical model predictions. Halo contamination at highly negative velocities is likely to be small. One reconciliation for this discrepancy between our observations and the tri-axial model may lie in the workings of the tri-axial model itself. Unlike other models considered, the tri-axial model does not reproduce the observed bifurcation in the Sgr stream (Belokurov et al. 2006). Although observationally untested, it is reasonable to suggest a bifurcation may result from a significant kinematic disruption. Such an effect could result in a broader kinematic distribution – similar to what we have observed – which is most notable at the stream edges.

There is further work required through observations and simulations to reconcile kinematic discrepancies. Typical examinations of the leading arm debris usually favour prolate halos and evidence along the trailing arm typically favours oblate halos (Helmi 2004; Martínez-Delgado et al. 2004; Law et al. 2005). Kinematic predictions of the LM10 tri-axial model reasonably match our observations, whereas the prolate model has been excluded as significant debris is not predicted in this edge of the stream. These observations along the Northern leading arm are the first which are not reproducible with the current prolate model of LJM05, contrary to previous groups who have surveyed closer to the leading arm debris.

A Metal-Poor Population Uncovered in Sagittarius Debris

Many groups have found the population of the Sgr core to possess a mean $[\text{Fe}/\text{H}] \sim -0.5 \text{ dex}$ (Cacciari et al. 2002; Bonifacio et al. 2004; Monaco et al. 2005). The observed metallicity gradient along the stream suggests that as the host circles the Milky Way the older, more metal-poor stars are preferentially stripped from the progenitor (Chou et al. 2007; Keller et al. 2010). In this region of the stream very few Sgr member metallicities have been reported. Vivas et al. (2005) found a mean metallicity of $\langle [\text{Fe}/\text{H}] \rangle = -1.77$ from spectra of 16 RR Lyrae stars along a nearby region of the Sgr leading arm. Similarly, Prior et al. (2009a) found $\langle [\text{Fe}/\text{H}] \rangle = -1.79 \pm 0.08$ for 21 type *ab* RR Lyrae stars in the region. This is somewhat expected since only the oldest, most metal-poor stars can form RR Lyraes.

Investigating the MDF of the Sgr debris requires an unbiased sample. Generally K-giants are excellent stellar candidates for such investigations as all stars go through this evolutionary phase whereas M-giants are consistently metal-rich. If we apply the metallicity gradient found by Keller et al. (2010, from M-giants) to these observed K-giants, we would expect an abundance mean near $\sim -1.2 \text{ dex}$ in this observed region. The metallicity distribution for our entire negative V_{GSR} sample is shown in Figure 2.6, and illustrates a metal-poor population. The mean of our distribution is $\langle [\text{Fe}/\text{H}] \rangle = -1.7 \pm 0.3 \text{ dex}$. If we include only the stars attributed to Feature A (as defined by the shaded region in Figure 2.3, between $-140 < V_{\text{gsr}} < -30 \text{ km s}^{-1}$) this value increases by only 0.04 dex; well within observational uncertainties. As a comparison, in a sample of metal-rich biased M-giants from the 2MASS data Chou et al. (2007) found a mean metallicity of $\langle [\text{Fe}/\text{H}] \rangle = -0.72 \text{ dex}$ for their best subsample in

the Northern leading arm of Sgr. Although there may be some halo contamination in our sample, in general our more metal-poor Feature A members have higher negative velocities, which is expected for Sgr stream members in this region.

It is likely that our observed K-giant sample is biased towards more metal-poor members. Given a typical distance of $r_\odot \sim 40$ kpc for the Sgr debris in this region (Belokurov et al. 2006), a 12 Gyr old Dartmouth (Dotter et al. 2008) isochrone with a metallicity of $[\text{Fe}/\text{H}] = -1.5$ falls directly within our target selection window. The more metal-rich isochrone with $[\text{Fe}/\text{H}] = -0.5$ does not pass through our selection range. This is consistent with our observed metallicities for Sgr. Although this does not prohibit the possibility of more metal-rich members within our sample, it implies that our distribution is biased towards the metal-poor end of the MDF. The tail of our Sgr distribution extends from -0.71 to -2.35 dex.

2.7.3. Feature B – The Virgo Stellar Stream

Another substructure which was distinguished from the general over-density of the VOD is the Virgo Stellar Stream (Duffau et al. 2006). Several RR Lyrae stars were noted with a common velocity of $V_{\text{GSR}} = 130 \text{ km s}^{-1}$ (Newberg et al. 2007; Prior et al. 2009b). Prior et al. (2009b) also measured metallicities of stars with this kinematic signature and found a mean $[\text{Fe}/\text{H}] = -1.95 \pm 0.1$ for the VSS, although this is based on RR Lyrae stars and therefore is potentially biased to the oldest, most metal-poor populations. The RR Lyrae sample from Duffau et al. (2006) found a $\langle [\text{Fe}/\text{H}] \rangle = -1.86$ with a much larger abundance spread of $\sigma = 0.40$, which was several times the relative uncertainty in individual values ($\sigma_{[\text{Fe}/\text{H}]} = 0.08$ dex). This led Duffau et al. (2006) to infer the progenitor of the VSS was likely a dSph galaxy, as a large dispersion in $[\text{m}/\text{H}]$ indicates self-enrichment and implies the structure is a galaxy and not an isolated stellar cluster. Although some globular clusters are also now known to contain multiple populations and sizeable $[\text{m}/\text{H}]$ dispersions, globular clusters in general have a much smaller dispersion than that observed here. Similar to Duffau et al. (2006), we also observe an abundance spread within this kinematic bin including two K-giants with mean kinematics and metallicities ($\langle V_{\text{GSR}} \rangle = 130 \pm 9 \text{ km s}^{-1}, \langle [\text{Fe}/\text{H}] \rangle = -2.0 \pm 0.16$) matching those found by Prior et al. (2009b). Monte-Carlo simulations reproduced these targets a mere $\sim 1\%$ in 10,000 simulations – highlighting their significance.

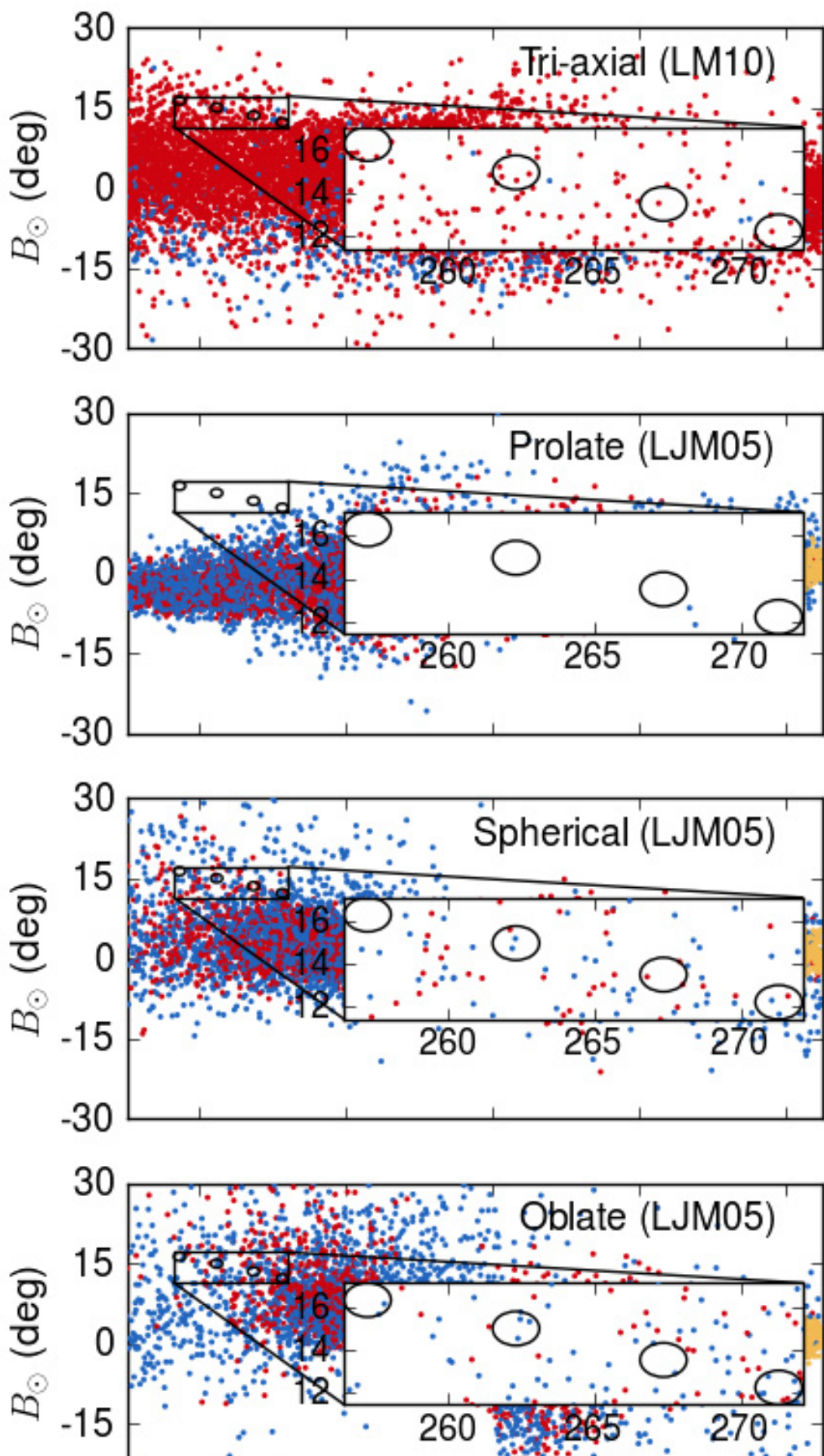
High resolution follow-up spectroscopy on these targets and other VSS candidates at higher metallicities in this kinematic range will provide crucial information about the origin of the VSS. Investigating $[\alpha/\text{Fe}]$ ratios in these candidates can constrain the mass of the VSS progenitor and discern whether the host was indeed a dSph (Venn et al. 2004; Casetti-Dinescu et al. 2009). Future observations are planned.

2.7.4. Feature C – Sagittarius debris?

The last significant kinematic substructure we identify in our data is Feature C. There are two peaks identified here at $V_{\text{GSR}} = 200$ and 240 km s^{-1} . These features cannot be explained by a smooth halo distribution. Newberg et al. (2007) identified a 4σ peak at $V_{\text{GSR}} = 200 \text{ km s}^{-1}$ in their sample of F turnoff stars centered on $(l, b) = (288^\circ, 62^\circ)$. Our nearest field to their

plate (Field B) hosts only one star associated with this peak; most of our stars are located within our most populated Field D. [Prior et al. \(2009a\)](#) also noted stars in this kinematic range and compiled a list of authors who have similarly observed such peaks (see [Sirko et al. \(2004\)](#); [Duffau et al. \(2006\)](#); [Starkenburg et al. \(2009\)](#)). [Prior et al. \(2009a\)](#) argue these stars may be associated with trailing debris of Sgr, as suggested by models (LJM05, LM10). Although this trailing debris would be much closer than the nearby visible leading arm, our observations support the interpretation by [Prior et al. \(2009a\)](#) as the metallicities are quite similar to the nearby Sgr debris.

This substructure has a range of metallicities. These metallicities were derived assuming a single distance modulus to the VOD/VSS. The abundance dispersion we observe is either representative, or these stars have a common metallicity and are dispersed along the line-of-sight. Unfortunately neither can be positively excluded without further observations. If these peaks are associated with the trailing debris of Sgr debris, they are likely to be further away than the VOD. On our scale that would make these stars more metal-rich than shown in Figure ???. However, the nearest trailing debris particles predicted from any best-fitting dark halo potential that could explain this kinematic peak occur at $\sim \Lambda_\odot = 310^\circ$; our observations range in longitude between $\Lambda_\odot = 256 - 273^\circ$. Whether this substructure is separate from Sgr debris or not remains equivocal. Nevertheless, the apparent metallicities of the Feature C stars are not inconsistent with those of a Sgr population given our results for Feature A and those of [Keller et al. \(2010\)](#).



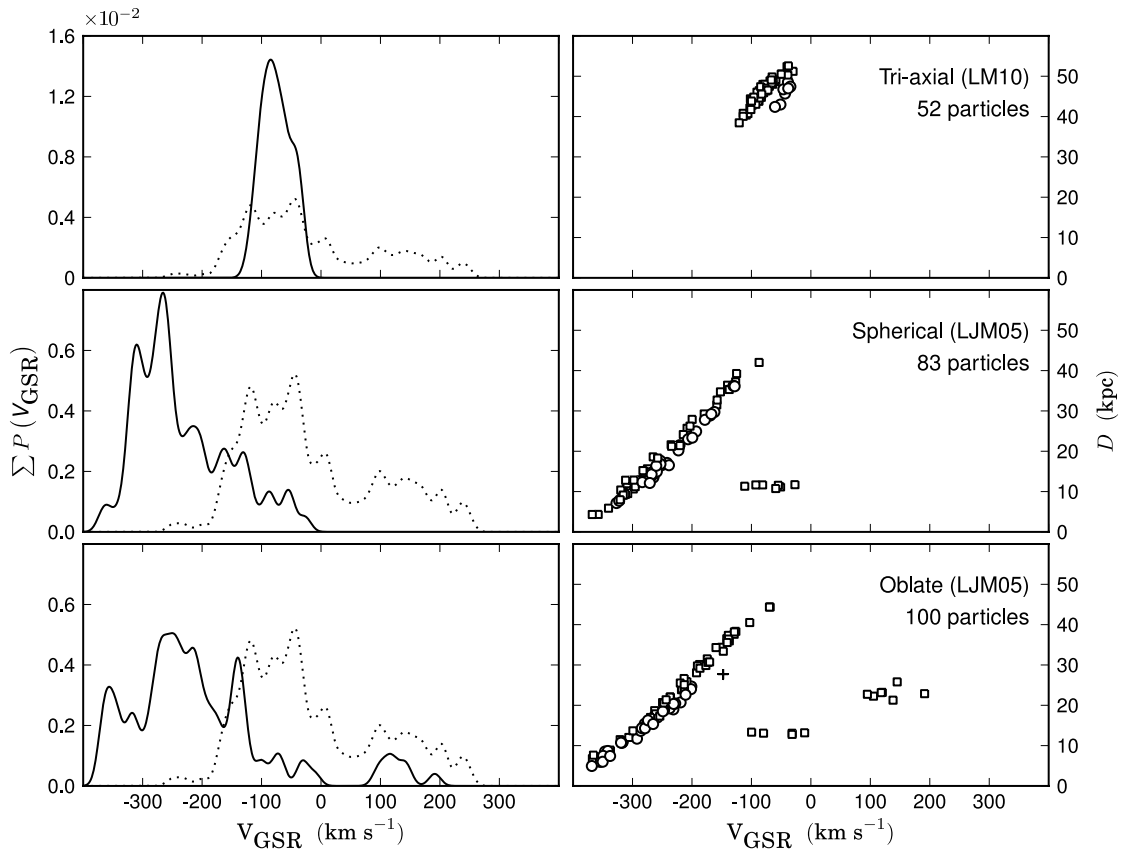


Figure 2.5 A generalised histogram (left) of the galactocentric rest frame velocities in our sample (dotted line) compared to the velocities (solid line) from the N -body models of LJM05, LM10 of particles within the same spatial coverage and distance range (up to $r_\odot \sim 60$ kpc) of our observed sample. Heliocentric distances for particles used to generate each velocity histogram are shown on the right. Particles are marked by their peri-centric passage. A plus (+) denotes debris from the current peri-centric passage by Sgr, circles (○) mark the previous passage, and squares (□) represent debris from two previous passages. The prolate model from LJM05 is not considered in this plot (see text).

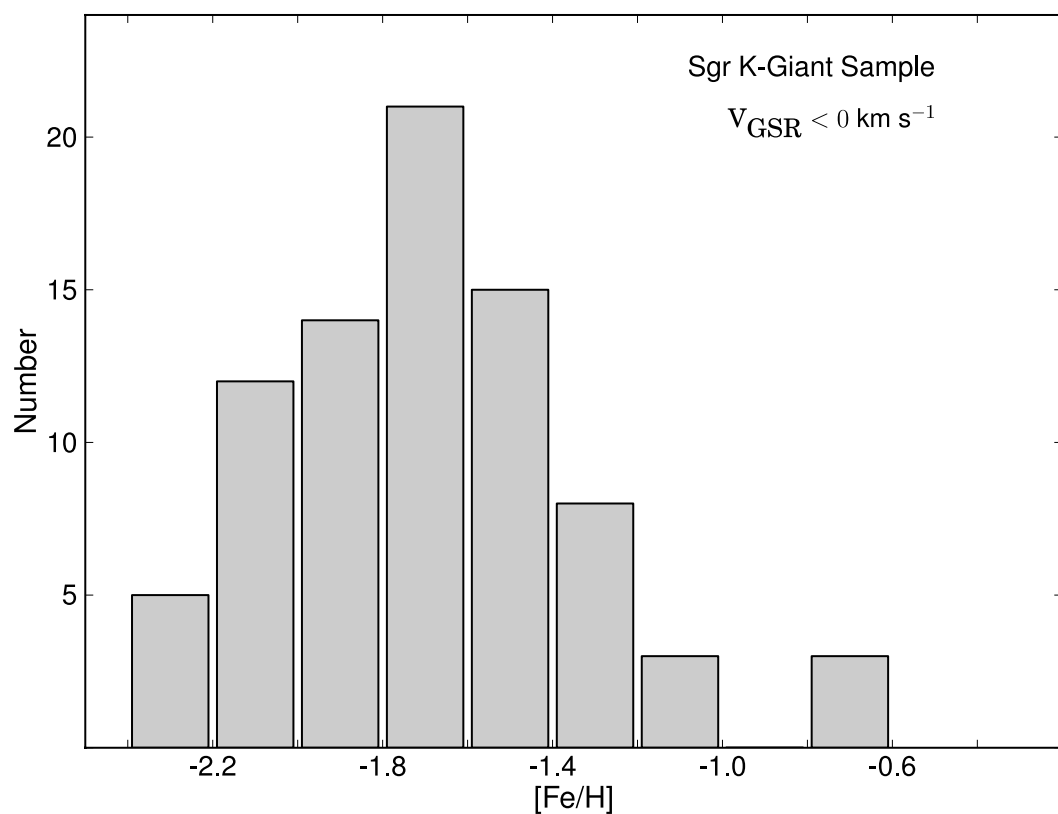


Figure 2.6 Metallicity histograms for K-giant members in our negative galactocentric velocity sample, which is largely populated by Sgr debris from the Northern leading arm.

2.8. Carbon Stars

In our sample we have identified five carbon stars. Our colour selection to select K-giants overlaps with where we would expect to find carbon stars. Although these stars were not specifically targeted, their surface densities are so low (≈ 1 per 50 deg^2 ; [Green et al. 1994](#)) that we would not expect them as a substantial contaminant. Although our sky coverage is small ($\sim 12.5 \text{ deg}^2$), the observed carbon star spatial density is $\sim 20x$ higher than expected. All five carbon stars are recognisable by the presence of distinctive 4737- and 5165 Å Swan C₂ bands.

Dwarf carbon stars exhibit a spectral signature which mimics that of a typical CH-type giant carbon star, however they have anomalous JHK colors ([Green et al. 1992](#)) and high proper motions. The existence of the 4300 Å CH G-band is representative of a CH-type carbon star, and is found in all five of our carbon stars. SDSS photometry for our stars match well with the F/G-type CH carbon stars identified by [Downes et al. \(2004\)](#), as seen in Figure 2.7. However these targets were not spectroscopically observed in the SDSS follow-up survey SEGUE. Through comparisons with previous carbon-type star catalogues ([Totten & Irwin 1998](#); [Downes et al. 2004](#); [Goswami et al. 2010](#)), the stars tabulated in Table ?? are previously unclassified carbon stars. This is largely because our objects are too faint to have been observed by previous spectroscopic carbon star surveys.

There is 2MASS photometry available for four of these stars. Of those, two stars (SDSS J125410.80-032744.0 and J125416.52-031437.6) exhibit anomalous JHK colors and significant ($> 3\sigma$) proper motions ([PPMXL Roeser et al. 2010](#)); characteristics of a dwarf carbon star. A third star also exhibits significant proper motion (SDSS J121740.94-001839.5), however JHK photometry is unavailable. The two remaining stars in our sample have JHK photometry characteristic of the F/G type CH carbon stars found by [Downes et al. \(2004\)](#) in their Faint High-Latitude Carbon (FHLC) star survey (Figure 2.7), and do not exhibit significant proper motion - which strongly suggests they are not dwarfs ([Green et al. 1994](#); [Deutsch 1994](#)).

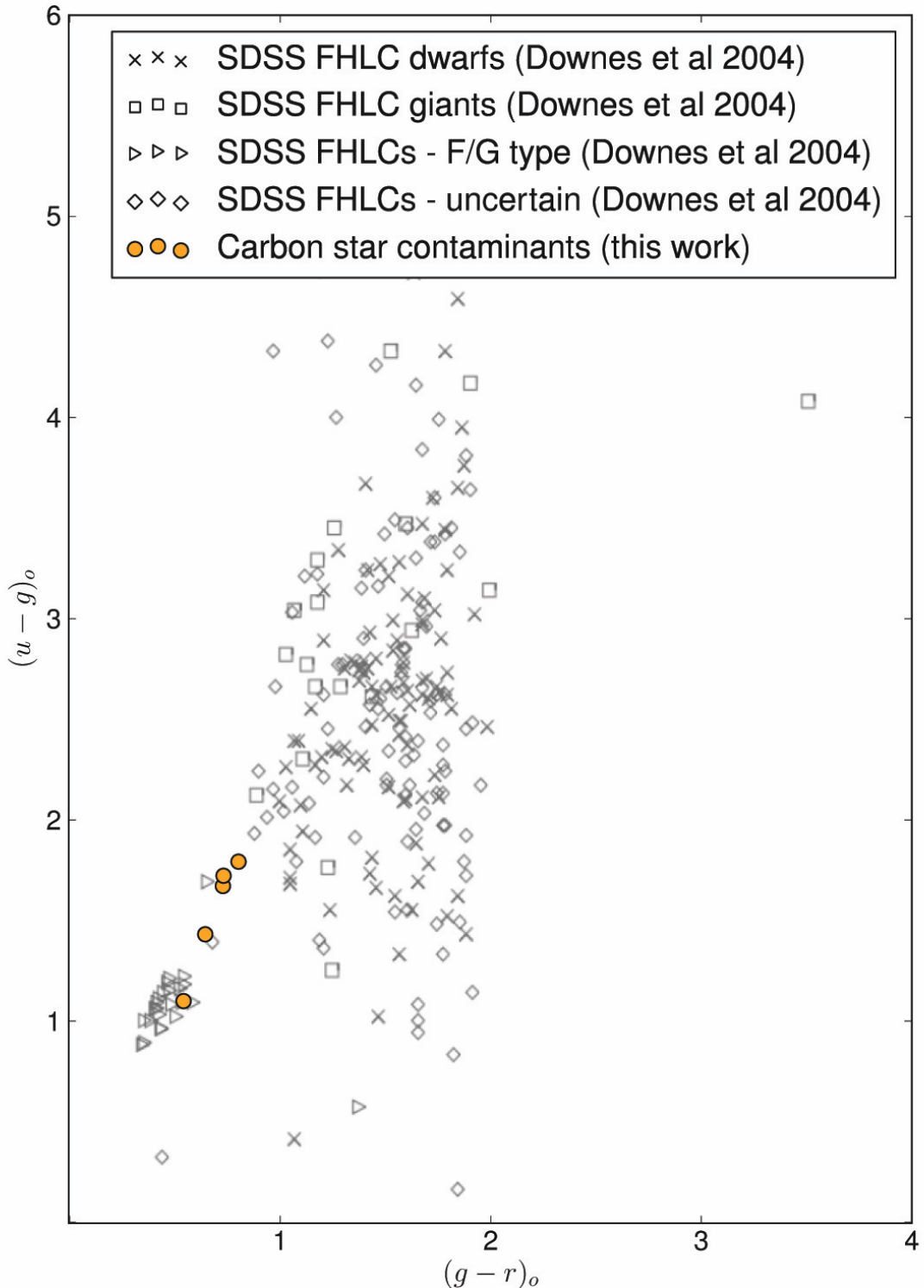


Figure 2.7 Sloan $u - g$ and $g - r$ colors for our carbon stars, and the identified carbon stars and classifications by Downes et al. (2004). Carbon stars identified in this work have been shaded for clarity.

2.9. Conclusions

We present spectroscopic observations of K-type stars in a region of the ‘Field of Streams’, where significant substructure is present. We utilise the gravity-sensitive Mg I triplet to

separate giants and dwarfs. Radial velocities and metallicities of 178 K-giants have been determined. We have recovered kinematic substructure found by other authors, which cannot be explained by a smooth halo distribution. Highly negative velocity signatures match those expected by the Sgr stream debris, and we also identify a group of K-giants with metallicities and kinematics which make them highly probable members of the Virgo Stellar Stream.

Stars in this region of the Sgr stream are kinematically sensitive to the shape of the Galactic dark halo. As such, we have compared our velocity distribution to the Sgr-Milky Way dark matter models of Law et al. (2005); Law & Majewski (2010). Typically, leading arm debris favour prolate models and trailing arm debris favour oblate models. A prolate dark halo predicts relatively little debris in our observed fields. If the spheroid is prolate and LJM05 presents an accurate representation, Sgr debris would not be expected to dominate our sample even if we were $\Delta B_\odot \sim 10^\circ$ closer to the great circle best-fit. However, Sgr debris is our most significant kinematic structure observed. No single model perfectly represents our data, although we find the more recent tri-axial model (LM10) best represents our observed kinematics.

Observed metallicities for K-giants in this region of the Sgr stream are notably lower than expected based on other Sgr samples, demonstrating the presence of a metal-poor population in the Sgr debris. Although isochrones indicate we are biased towards metal-poor members at these distances, these stars are unequivocally Sgr in origin. Metallicity gradients reported, suggest a mean of $\langle [\text{Fe}/\text{H}] \rangle \sim -1.2$, whereas our population has $\langle [\text{Fe}/\text{H}] \rangle = -1.7 \pm 0.3$ dex. Previously reported abundances in this region have been ascertained from observing RR Lyrae stars (where the mean metallicity found was $\langle [\text{Fe}/\text{H}] \rangle \sim -1.7$ dex) or from observing M-giants (where $\langle [\text{Fe}/\text{H}] \rangle \sim -0.7$ dex was reported). In both scenarios the measurements are reasonable with what we would expect from each particular stellar population. Thus the sample presented here is more representative of the complete MDF, and less susceptible to age or metallicity biases. These observations also demonstrate that the Sgr stream likely hosts a substantially larger abundance range than previously found, including a previously un-detected metal-poor population of K-giants.

CHAPTER 3

Hunting the Parent of the Orphan Stream

Parts of this chapter have been previously published as ‘Hunting the Parent of the Orphan Stream: Identifying Stream Members from Low-Resolution Spectroscopy’, Casey, A. R., Da Costa, G., Keller, S. C., Maunder, E., 2013, ApJ, 764, 39C. The work is presented here in expanded and updated form.

3.1. Introduction

We present candidate K-giant members in the Orphan Stream which have been identified from low-resolution data taken with the AAOmega spectrograph on the Anglo-Australian Telescope. From modest S/N spectra and independent cuts in photometry, kinematics, gravity and metallicity we yield self-consistent, highly probable stream members. We find a revised stream distance of 22.5 ± 2.0 kpc near the celestial equator, and our kinematic signature peaks at $V_{GSR} = 82.1 \pm 1.4$ km s⁻¹. The observed velocity dispersion of our most probable members is consistent with arising from the velocity uncertainties alone. This indicates that at least along this line-of-sight, the Orphan Stream is kinematically cold. Our data indicates an overall stream metallicity of $[Fe/H] = -1.63 \pm 0.19$ dex which is more metal-rich than previously found and unbiased by spectral type. Furthermore, the significant metallicity dispersion displayed by our most probable members, $\sigma([Fe/H]) = 0.56$ dex, suggests that the unidentified Orphan Stream parent is a dSph satellite. We highlight likely members for high-resolution spectroscopic follow-up.

3.2. Introduction

The Milky Way stellar halo has partly formed through the accretion of satellites that are disrupted by tidal forces as they fall into the Galaxy’s potential. Stars which were once gravitationally bound to the satellite are distributed along the progenitor’s orbit in leading and trailing streams of stars. The velocities of stars in the stream are sensitive to the shape of the dark matter halo, allowing us to constrain the Milky Way potential and reconstruct the formation history of the Galaxy. The level of accreted substructure in the Milky Way has only

recently become apparent through multi-band photometric surveys like the Sloan Digital Sky Survey (SDSS). The more prominent of the detectable substructures, like Sagittarius, have been well-studied. One of the more prominent – yet less studied – substructures is that of the Orphan Stream.

The Orphan Stream was independently detected by both ? and ?, and is distinct from other substructures in the halo. The stream stretches over 60° in the sky, has a low surface brightness, and a narrow stream width of only $\sim 2^\circ$. As the name suggests, the parent object largely remains a mystery. The stream extends past the celestial equator – outside the SDSS footprint – but has not been detected in existing southern surveys (?). Whilst the parent system remains elusive, significant effort has been placed on associating the stream with known Milky Way satellites (????). In contrast, there has been relatively limited observational work on the Orphan Stream itself other than the original discovery papers (???) and the work of ?. This is largely to be expected given the absence of deep multi-band photometry in the southern sky and the low total luminosity of the stream. This makes it difficult to reliably separate Orphan Stream members from halo stars. Understanding the full extent of the stream awaits the SkyMapper and Pan-STARRS photometric surveys (??).

As ? point out, there is a natural observational bias towards more massive and recent mergers like Sagittarius. Consequently, the fainter end of this substructure distribution has yet to be fully recovered, or thoroughly examined. Interestingly, there are indications that some fainter substructures like the Orphan Stream and the Palomar 5 tidal tails (?) have orbits which seem to be best-fit by Milky Way models with nearly 60% less mass (?) than generally reported by ? and ?. Such a discrepancy in the mass of the Milky Way is troublesome. More complete photometric and kinematic maps of these low total luminosity streams may provide the best test as to whether this mass discrepancy is real, or an artefact of incomplete observations. Whilst the full spatial extent of the Orphan Stream remains unknown, we can examine the detailed chemistry of its members, investigate the stream history, and make predictions about the nature of the progenitor.

In this paper we present a detailed, self-consistent analysis to identify K-giant members of the Orphan Stream. Using our selection method we have catalogued the locations of nine highly probable Orphan Stream candidates, all worthy of high-resolution spectroscopic follow up. In the following section we outline our photometric target selection. In §3.4 we describe the low-resolution spectroscopic observations. The data analysis, including stream identification, is discussed in §3.5 and in §3.6 the conclusions, predictions and future work are presented.

3.3. Target Selection

We have targeted K-giant members of the Orphan Stream in order to investigate their detailed chemistry. Because K-giants are difficult to unambiguously detect from photometry alone, low-resolution spectroscopy is required to estimate stellar parameters and determine radial velocities. The Orphan Stream has an extremely low spatial over-density, which makes it difficult to separate stream members from halo stars. However, there is a well described distance gradient along the stream (??) which provides an indication on where we should focus our spectroscopic efforts.

The Orphan Stream is closest to us in two locations on the edge of the SDSS footprint: at the celestial equator (?), and along outrigger SEGUE Stripe 1540 (?). These two locations are unequivocally the best place to recover bright stream members. We have targeted two fields centered on $(\alpha, \delta) = (10:48:15, 00:00:00)$ and $(10:48:15, -02:30:00)$, and employed a combination of colour cuts with the SDSS DR 7 (?) data set in order to identify likely K-giants:

$$0.6 < (g - i)_0 < 1.7 \quad (3.1)$$

$$-15(g - i)_0 + 27 < g_0 < -3.75(g - i)_0 + 22.5 \quad (3.2)$$

$$15 < i_0 < 18 \quad (3.3)$$

Given our colour selection we expect to recover giants and contaminating dwarfs. Although the 2MASS *JHK* colours can help to separate dwarfs and giants, our target K-giants stars are too faint to be detected in the 2MASS catalogue.

3.4. Observations

Observations took place on the Anglo-Australian Telescope using the AAOmega spectrograph in April 2009. AAOmega is a fibre-fed, dual beam multi-object spectrograph which is capable of simultaneously observing spectra of 392 (science and sky) targets across a 2° field of view. We used the 5700 Å dichroic in combination with the 1000I grating in the red arm, and the 580V grating in the blue arm. This provides a spectral coverage between $800 \leq \lambda \leq 950$ nm in the red at $\mathcal{R} \approx 4400$, and between $370 \leq \lambda \leq 580$ nm with a lower spectral resolution of $\mathcal{R} \approx 1300$ in the blue.

The data were reduced using the standard 2DFDR reduction pipeline¹. After flat-fielding, throughput calibration for each fibre was achieved using the intensity of skylines in each fibre. The median flux of dedicated sky fibres was used for sky subtraction, and wavelength calibration was performed using ThAr arc lamp exposures taken between science frames. Three thirty minute science exposures were median-combined to assist with cosmic ray removal. The median S/N obtained in the red arm for our fields is modest at 35 per pixel, although this deteriorates quickly for our fainter targets. With the presence of strong Ca II triplet lines in the red arm we are able to ascertain reliable radial velocities and reasonable estimates on overall metallicity (?), and references therein). Our spectral region also includes gravity-sensitive magnesium lines: Mg I at 8807 Å, and the Mg Ib 3p-4s triplet lines at ~5178 Å. As we demonstrate in the next section, these lines are sufficient to discriminate dwarfs from giants even with weak signal.

The blue and red arm spectra were normalised using a third order cubic spline after multiple iterations of outlier clipping. We used defined knot spacings of 20 nm in the red arm, and 5 nm in the blue arm in order to accommodate often poor S/N, and varying strengths of molecular band-heads.

¹http://www.ao.gov.au/2df/aaomega/aaomega_2dfdr.html

3.5. Analysis & Discussion

We have employed a combination of separate criteria to identify likely Orphan Stream members: kinematics, a giant/dwarf indication from Mg I lines, and selecting stars with consistent metallicities derived from both isochrone fitting and the strength of the Ca II triplet lines. Each criteria is discussed here separately.

3.5.1. Kinematics

Radial velocities were measured by cross-correlating our normalised spectra against a K-giant synthetic template with a temperature of 4500 K, $\log g = 1.5$ and $[M/H] = -1.5$ across the range $845 \leq \lambda \leq 870$ nm. Heliocentric velocities were translated to the galactic rest frame by adopting the local standard of rest velocity as 220 km s^{-1} towards $(l, b) = (53^\circ, 25^\circ)$ (??)².

Figure ?? shows a histogram of our galactocentric velocities, compared to the predicted smooth line-of-sight velocity distribution for this region from the Besançon model (?). We have selected particles from the Besançon model using the same criteria outlined in §3.3 after employing the ? colour transformations. It is clear that our target selection has yielded mostly nearby disk dwarf stars with $V_{GSR} \approx -120 \text{ km s}^{-1}$.

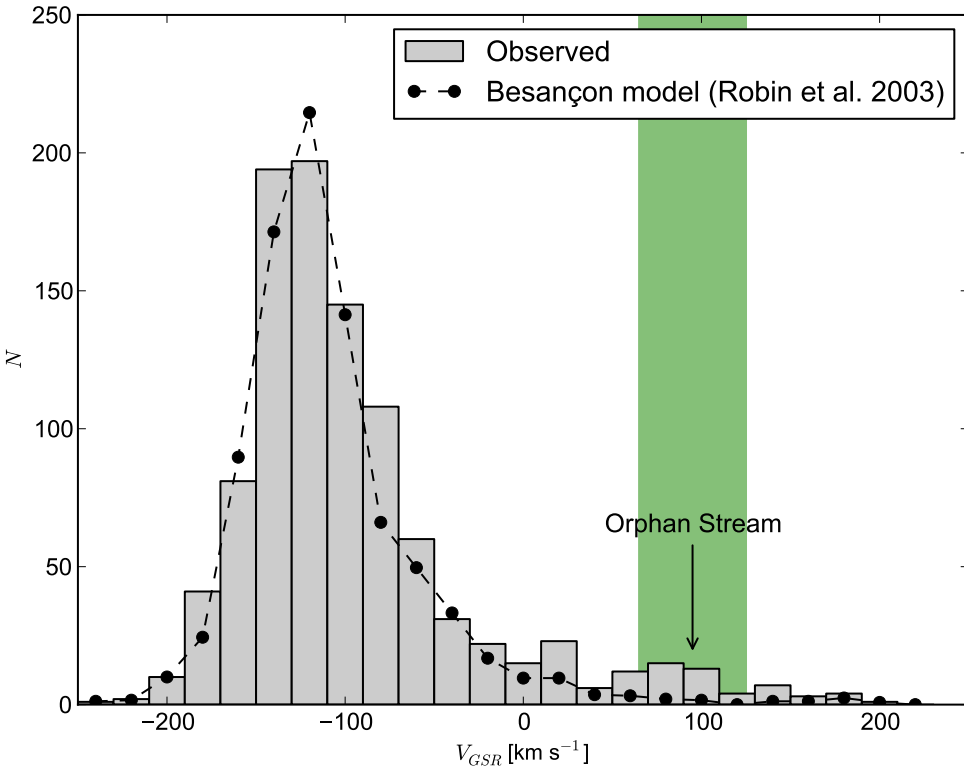


Figure 3.1 Galactocentric rest frame velocities for stars in both our observed fields (grey), and predicted Besançon velocities which have been scaled to match our observed sample size. The expected kinematic signature from ? for the Orphan Stream is highlighted, as is our kinematic selection window (green).

²Where $V_{GSR} = V_{HELIO} + 220 \sin l \cos b + 16.5 \times [\sin b \sin 25^\circ + \cos b \cos 25^\circ \cos(l - 53^\circ)]$

In a nearby ($\Delta\Lambda_{Orphan} \sim 4^\circ$) region of the stream, ? detected the Orphan Stream with a $V_{GSR} = 101.4 \text{ km s}^{-1}$ from BHB stars. Differences in accounting for the local standard of rest between this work and ? means that this corresponds to approximately 95 km s^{-1} on our V_{GSR} scale. This is discussed further in §3.5.5. The expected Orphan Stream kinematic peak is labelled in Figure ???. There is no obvious sharp kinematic peak representative of the Orphan Stream in our sample. From kinematics alone, our targets appears largely indistinguishable from a smooth halo distribution. To isolate potential Orphan Stream members we have nominated a relatively wide selection criteria between $65 \leq V_{GSR} \leq 125 \text{ km s}^{-1}$ (shown in Figure ??), which yields 28 Orphan Stream candidates. The typical uncertainty in our velocities is $\pm 5.0 \text{ km s}^{-1}$.

3.5.2. Dwarf/Giant Discrimination

We have measured the equivalent width of the gravity-sensitive Mg I line at 8807 \AA to distinguish dwarfs from giants (?). At a given temperature (or $g - r$) and metallicity, giant stars present narrower Mg I absorption lines than their dwarf counterparts. Given the target selection, our sample is likely to contain many more dwarfs than giants (e.g. see ? where a similar colour selection was employed). In some cases no Mg I 8807 \AA line was apparent, so an upper limit was estimated based on the S/N of the spectra. In these cases the candidate was considered a “non-dwarf” because we cannot exclusively rule out a metal-poor sub-giant with this criteria alone. For these purposes we are only looking for a simple indication as to whether a star is likely a dwarf or not.

Figure ?? illustrates the trend with $EW_{\lambda 8807}$ against SDSS de-reddened³ $g - r$, illustrating the dominant upper dwarf branch we wish to exclude. Giant stars populate the lower, sparser branch. A separation line has been adopted to distinguish dwarfs from giants, and is shown in Figure ???. If we were to place this line higher, the total number of true giant stars may increase, but the dwarf contamination rate will rise dramatically. A compromise must be made between the rate of giant recoverability and the dwarf contamination. Our dwarf/giant separation line lies just below the main dwarf population. On its own, this dwarf/giant separation line would typically result in far too many dwarf contaminants. However, we are employing selections on multiple observables (kinematics, metallicity, proper motions) in order to refine our Orphan Stream giant sample.

This dwarf/giant separation method was also employed using the total equivalent width of the Mg Ib triplet lines. Both analyses were entirely consistent with each other: essentially the same candidate list was found using both techniques. However, given slightly poorer signal at the Mg Ib triplet, we were forced to adopt many more upper limits than when using the 8807 \AA line. Because we classify all upper limits as being “non-dwarfs” (i.e. potential giants), we deduced a slightly larger candidate sample for the Mg Ib analysis, which was primarily populated by upper limits. In conclusion, we found the Mg I line at 8807 \AA appeared to be a more consistent dwarf discriminant given our weak S/N – particularly for our fainter stars. Thus, we have used the 8807 \AA Mg I selection throughout the rest of our analysis.

Our dwarf/giant separation line in Figure ?? yields 425 potential giants. Upon taking the intersection of our kinematic and gravity selections, we find 20 stars that appear to be likely

³All magnitudes presented in this letter are de-reddened using the ? dust maps.

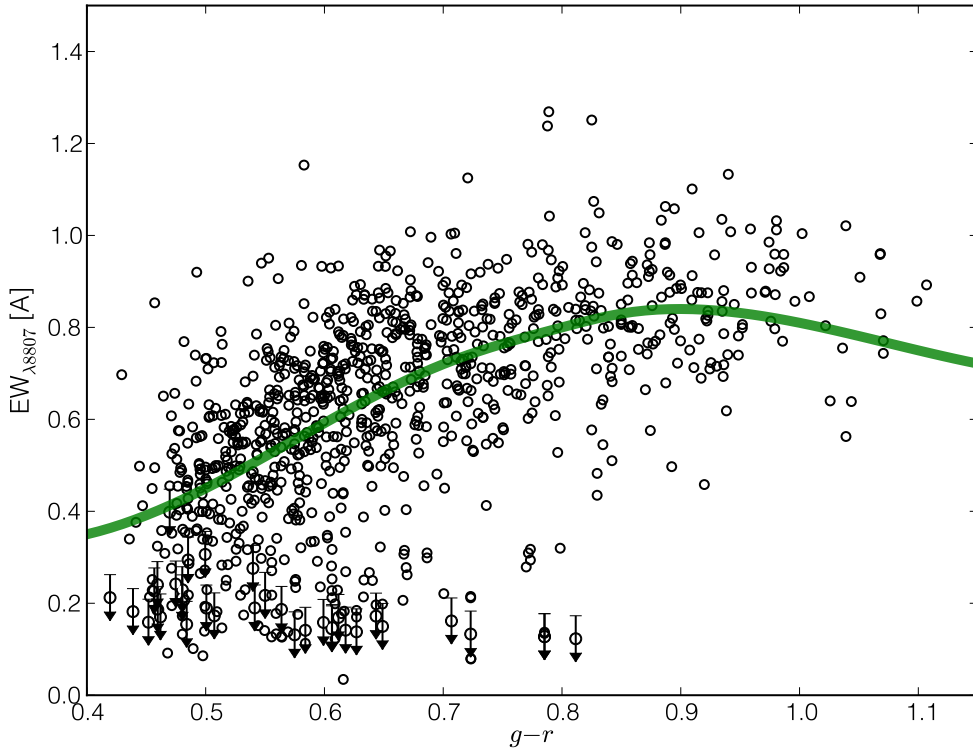


Figure 3.2 SDSS $g-r$ against the measured equivalent width of the Mg I transition at 8807 Å. Dwarf contaminants occupy the more populous upper branch. Our separation line between dwarfs and giants is shown in green.

Orphan Stream giants.

3.5.3. Metallicities

We have measured the metallicities for the stars that meet our kinematic and surface gravity criteria in two ways: with the strength of their Ca II triplet lines, and by isochrone-fitting. After correcting for luminosity, the equivalent width of the Ca II triplet lines provide a good indication of the overall metallicity of a RGB star (?). We have employed the ? relationship and corrected for luminosity in g against the horizontal branch magnitude at $g_{HB} = 17.1$ (?). Strictly speaking, the Ca II-[Fe/H] calibration is only valid for stars brighter than the horizontal branch, although the relationship only becomes significantly inappropriate near $g - g_{HB} \sim +1$ (?). Many of our candidates are fainter than this valid luminosity range, and therefore they should not be excluded solely because of their derived metallicities, as these could be uncertain. Stars fainter than g_{HB} will have slightly lower metallicities than predicted by our Ca II-[Fe/H] relationship, and for these stars we will only use metallicities to assign a relative qualitative likelihood for stream membership.

Given a distance estimate to the Orphan Stream, we can also deduce a star's metallicity through isochrone fitting. We have used a 10 Gyr ? isochrone at 21.4 kpc (?) and found metallicities for all 20 likely stream members from their best-fitting isochrone. Derived metallicities from Ca II line strengths and isochrone fitting that are consistent (within ± 0.3 dex) indicates these measurements are reliable, and that these stars are indeed at a

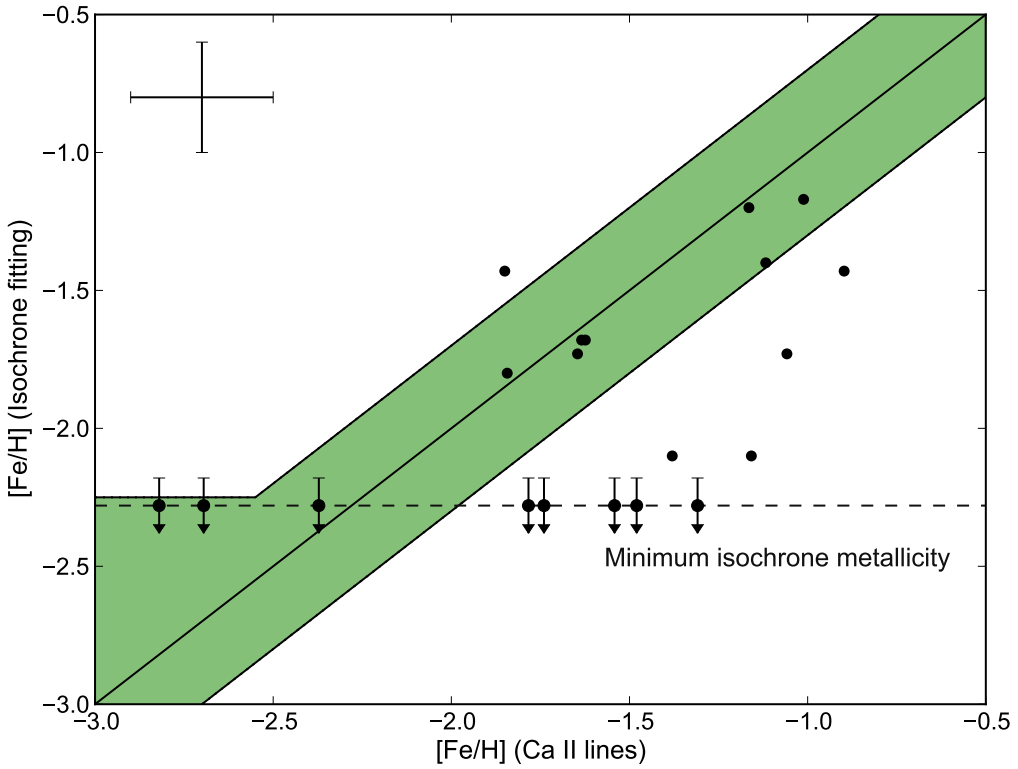


Figure 3.3 Metallicities from the Ca II triplet lines versus those found from fitting isochrones to the 20 stars that meet our kinematic and surface gravity criteria. Both abundance determinations imply these stars are RGB members of the Orphan Stream at a distance of ~ 21.4 kpc (?). Consistency between these methods indicates highly likely stream membership (shaded region). The minimum isochrone [Fe/H], and a representative uncertainty of 0.2 dex for abundance measurements is shown.

distance of ~ 21.4 kpc. We find ten highly likely stream members with consistently derived metallicities. They fall within the shaded region illustrated in Figure ??.

A final metallicity value for each star has been adopted based on the quality of our [Fe/H] measurements. These values are tabulated in Table 3.1. From our highly likely stream members we find an overall stream metallicity of $[Fe/H] = -1.63$ with a dispersion of $\sigma = 0.56$ dex. This abundance spread is larger than typically seen in globular cluster stars and is more representative of the chemical spread seen in dSph satellites (e.g., ?).

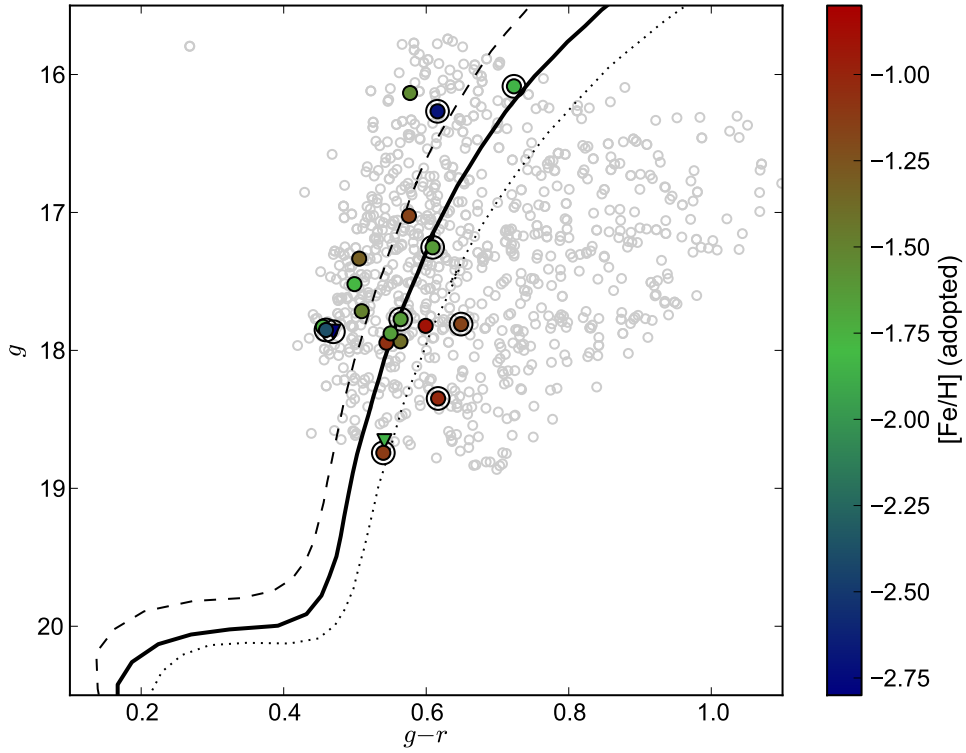


Figure 3.4 Color magnitude diagram showing our observed candidates (grey). Observations fulfilling kinematic and gravity cuts are colored by their metallicity, and those with upper limits for surface gravity are marked as triangles (∇). Highly probable stream members (see text) are circled. Relevant 10 Gyr ? isochrones at $[\text{Fe}/\text{H}] = -1.5$ (dotted), -2.0 (dashed) at 21.4 kpc (?) are shown, as well as our best-fitting 10 Gyr isochrone of $[\text{Fe}/\text{H}] = -1.63$ at 22.5 kpc (solid).

3.5.4. Proper Motions & Distances

We have found proper motions for 19 of our candidates in the PPMXL proper motion catalogue (?). One highly probable candidate (OSS-13 in Table 3.1) has a listed proper motion that is different from that of the other nine highly likely members at the 6σ level. Consequently, we have reduced the membership likelihood of this star from “High” to “Medium”. Given the uncertainties in proper motions, we cannot reliably alter the membership probability for any other candidate.

Since our Orphan Stream giants cover a wide evolutionary range along the giant branch (Figure ??), we are in a good position to revise the distance estimate to the stream. Given a 10 Gyr ? isochrone at $[\text{Fe}/\text{H}] = -1.63$, we find a best-fitting distance to the stream of 22.5 ± 2.0 kpc at $(l, b) = (250^\circ, 50^\circ)$. This isochrone is shown in Figure ???. Our derived distance is in reasonably good agreement with the measurement of 21.4 ± 1.0 kpc independently deduced by ? and ?.

3.5.5. Comparison with ?

? traced the Orphan Stream using BHB stars selected from the SEGUE survey, allowing them to derive an orbit for the stream and make a strong prediction for the location of the

Table 3.1 Identified Orphan Stream Candidates

Star Name	α (J2000)	δ (J2000)	g	$g - r$	μ_α (mas yr $^{-1}$)	μ_δ (mas yr $^{-1}$)	V_{GSR} (km s $^{-1}$)	$EW_{\lambda 8807}$ (mÅ)	[Fe/H] $_{Ca}$ (dex)	[Fe/H] $_{iso}$ (dex)	[Fe/H] 4 (dex)	S
OSS-1	10:46:21.9	+00:43:21.8	17.52	0.50	4.1 ± 4.5	-34.0 ± 4.5	73.3 ± 9.3	0.273	-1.78	<-2.28	-1.78	M
OSS-2	10:46:29.3	-00:19:38.5	17.77	0.56	-1.7 ± 4.3	-2.2 ± 4.3	78.4 ± 5.2	0.126	-1.63	-1.68	-1.63	M
OSS-3	10:46:50.4	-00:13:15.6	17.33	0.51	1.8 ± 4.3	-4.6 ± 4.3	77.0 ± 4.0	0.416	-1.31	<-2.28	-1.31	M
OSS-4	10:47:06.1	-01:56:03.9	18.74	0.54	-6.3 ± 4.9	4.6 ± 4.9	74.9 ± 17.6	0.452	-1.12 ⁵	-1.40	-1.40	M
OSS-5	10:47:15.0	-03:15:03.9	18.66	0.54	-8.2 ± 5.2	1.7 ± 5.2	109.5 ± 9.0	<0.19	-1.85 ^b	-1.43	-1.43	M
OSS-6	10:47:17.6	+00:25:07.7	16.09	0.72	-0.8 ± 4.0	-5.2 ± 4.2	79.2 ± 3.3	0.212	-1.84	-1.80	-1.84	M
OSS-7	10:47:29.1	-02:02:22.6	17.86	0.47	93.2 ± 29.8	<0.40	-2.82	<-2.28	-2.82	M
OSS-8	10:47:30.1	-00:01:24.5	17.25	0.61	-4.0 ± 4.2	-5.2 ± 4.2	83.6 ± 3.5	0.123	-1.62	-1.68	-1.62	M
OSS-9	10:48:20.9	+00:26:34.4	17.88	0.55	-8.1 ± 4.3	-5.4 ± 4.3	118.9 ± 11.7	0.467	-1.65	-1.73	-1.65	M
OSS-10	10:48:27.8	+00:55:24.0	17.72	0.51	-14.4 ± 4.6	-5.3 ± 4.6	124.5 ± 6.7	0.182	-1.48	<-2.28	-1.48	M
OSS-11	10:48:31.9	+00:03:35.7	17.02	0.58	-3.6 ± 4.1	-7.7 ± 4.1	105.1 ± 5.1	0.234	-1.12	-2.10	-1.12	M
OSS-12	10:48:44.4	-02:53:08.8	18.35	0.62	-3.4 ± 4.7	-1.8 ± 4.7	108.2 ± 9.0	0.183	-1.01 ^b	-1.17	-1.17	M
OSS-13	10:48:46.9	-00:32:27.8	17.85	0.46	-28.4 ± 4.8	-12.3 ± 4.8	109.3 ± 8.1	0.324	-2.37	<-2.28	-2.37	M
OSS-14	10:49:08.3	+00:02:00.2	16.27	0.62	4.9 ± 4.0	-6.0 ± 4.0	81.5 ± 4.6	0.034	-2.70	<-2.28	-2.70	M
OSS-15	10:49:13.4	+00:04:03.8	17.83	0.46	3.4 ± 4.7	-6.8 ± 4.7	65.3 ± 5.4	0.252	-1.74	<-2.28	-1.74	M
OSS-16	10:50:13.1	+00:33:52.7	16.13	0.58	-3.4 ± 4.0	-7.7 ± 4.0	94.7 ± 5.1	0.391	-1.54	<-2.28	-1.54	M
OSS-17	10:50:24.2	-01:49:05.4	17.94	0.54	3.4 ± 4.6	-2.2 ± 4.6	109.9 ± 25.4	0.151	-1.06	-1.73	-1.06	M
OSS-18	10:50:33.8	+00:12:19.1	17.82	0.60	-7.4 ± 5.0	-3.3 ± 5.0	97.5 ± 5.9	0.596	-0.90	-1.43	-0.90	M
OSS-19	10:51:19.7	+00:05:15.5	17.81	0.65	4.2 ± 4.7	-11.8 ± 4.7	82.7 ± 5.0	0.198	-1.16	-1.20	-1.16	M
OSS-20	10:51:35.4	+00:00:46.4	17.93	0.56	-0.5 ± 4.5	-3.0 ± 4.5	66.7 ± 8.7	0.128	-1.38	-2.10	-2.10	M

undiscovered progenitor. Their closest stream detection to this study is at $\Lambda_{Orphan} = 18.4^\circ$, approximately $\Delta\Lambda_{Orphan} \sim 4^\circ$ away from our fields. At this location, ? found the velocity of the stream to be $V_{GSR} = 101.4 \pm 8.9$ km s $^{-1}$ based on 12 BHB stars. We note that this is ~ 95 km s $^{-1}$ on our scale, given the differences in accounting for the local standard of rest. The velocities and metallicities of our ‘High’ and ‘Medium’ probability candidates are illustrated in Figure ???. Although we recover some candidates with velocities up to $V_{GSR} \sim 110$ km s $^{-1}$, our kinematic distribution peaks near $V_{GSR} \sim 85$ km s $^{-1}$, roughly 10 km s $^{-1}$ lower than that of ?.

There is a known velocity gradient along the Orphan Stream which can account for this discrepancy. As Λ_{Orphan} increases towards the edge of the SDSS boundary, galactocentric velocity quickly decreases. For the Orphan Stream detection in the outrigger SEGUE Strip 1540 at $\Lambda_{Orphan} = 36^\circ$, ? find $V_{GSR} = 38$ km s $^{-1}$. This work presents likely Orphan Stream K-giant candidates at $\Lambda_{Orphan} \sim 23^\circ$. Given the velocity gradient reported by ?, a galactocentric velocity of 80 – 85 km s $^{-1}$ (on our scale) is perfectly reasonable. We note that since the velocities of BHB stars can have significant uncertainties, it was practical for us to assume a wide initial selection in kinematics to identify potential members.

The adopted metallicities of our Orphan Stream candidates are generally higher than those found by ?. Our highly likely stream members have a mean metallicity of [Fe/H] = -1.63, with a dispersion of $\sigma = 0.56$ dex. As illustrated in Figures ?? and ??, there are two very metal-poor candidates which largely drive this dispersion, but we have no reason to suspect they are non-members. The ? sample contains 37 BHB stars identified over a 60° arc on the sky, and has a peak metallicity at [Fe/H] = -2.10 ± 0.10. The closest detection bin in the ? sample was the most populous, yielding 7 BHB stars. For comparison, we identify 9 giant stars across $\sim 4^\circ$. Given BHB stars are known to trace a somewhat more metal-poor

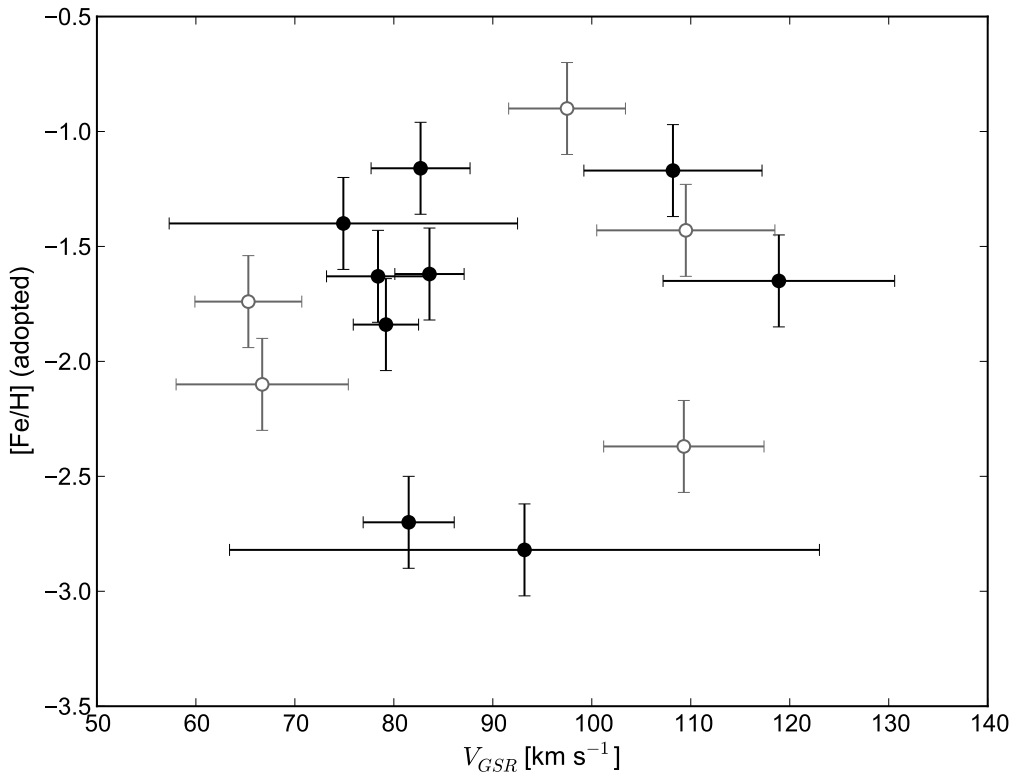


Figure 3.5 Galactocentric velocities and adopted metallicities for the highest likely Orphan Stream members (black ●), and those with probabilities assigned as “Medium” (grey ○; see text).

population, and we are calculating statistics with marginal sample sizes, we conclude that the accuracy of these two metallicity distributions are not mutually exclusive. It is entirely possible that we are sampling the same distribution, but a larger sample size is required.

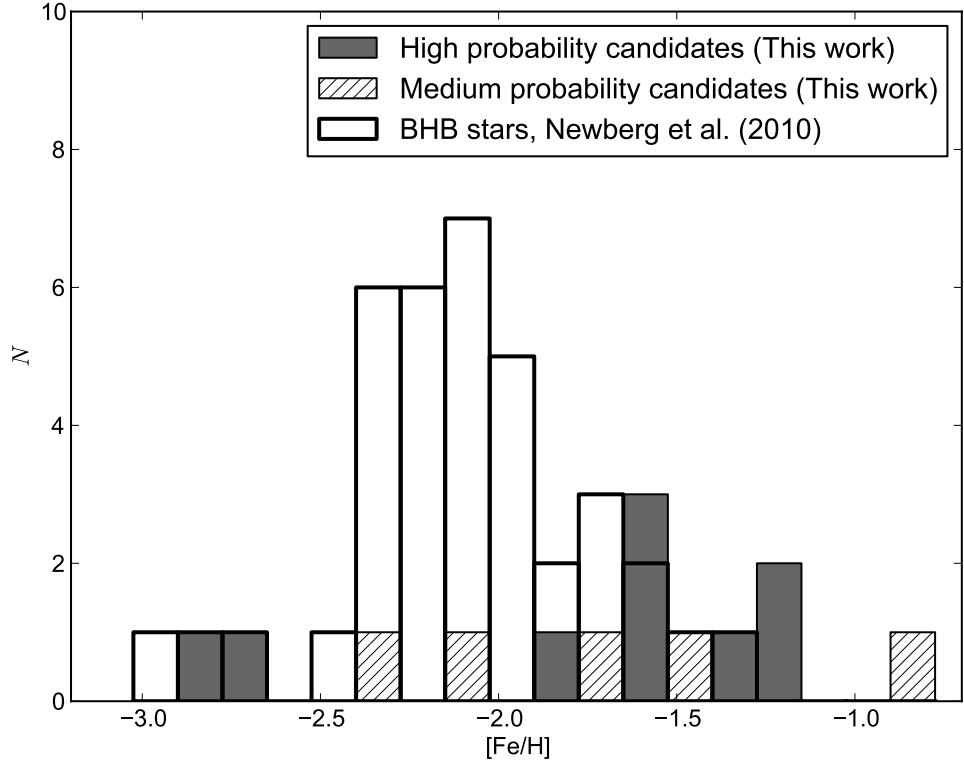


Figure 3.6 Observed metallicity distribution function for the Orphan Stream candidates identified here, with comparisons to the distribution found by ? from BHB stars.

3.6. Conclusions

We have presented a detailed analysis to isolate individual Orphan Stream K-giants from low-resolution spectroscopy using a combination of photometric, kinematic, gravity, metallicity, and proper motion information. Although each individual criterion is likely to induce some level of contamination, their intersection reveals nine highly probable, self-consistent, Orphan Stream K-giants. We deduce a median stream metallicity of $[Fe/H] = -1.63 \pm 0.19$ and find an intrinsically wide metallicity spread of $\sigma = 0.56$ dex, indicative of a dSph origin. Unlike other stellar tracers, K-type giants can exist at all metallicities, hence our derived metallicity spread is likely representative of the true stream metallicity distribution function. Recall that the metallicity determination was performed after kinematic and gravity cuts, and three of our most probable members lay perfectly on a 10 Gyr isochrone of $[Fe/H] = -1.63$. However, it is clear that more data is required to fully characterize the stream metallicity distribution function. Our data indicate a distance to the stream of 22.5 ± 2.0 kpc at $(l, b) = (250^\circ, 50^\circ)$, in agreement with that deduced by ? and ?.

Given the stream orbit derived by ?, they excluded all possible known halo objects except for the dissolved star cluster, Segue 1. ? obtained spectroscopy for six members in Segue 1 and found an extremely wide metallicity dispersion: from < -3.4 to -1.63 dex. On the basis of the extremely low metallicity in the cluster and the wide chemical dispersion, they conclude that Segue 1 is a dwarf spheroidal galaxy. Although the data presented here

indicates the Orphan Stream progenitor is a disrupted dwarf spheroidal galaxy, we cannot reliably associate Segue 1 as the parent without additional observational data.

If the Orphan Stream continues through SEGUE Stripe 1540 at $(l, b) = (271^\circ, 38^\circ)$ as ? found, then the stream is even closer there than in the region analysed here. Thus, if our observations and analyses are repeated at $(271^\circ, 38^\circ)$, we predict K-giant stream members of brighter apparent magnitude will be recovered.

Using a maximum-likelihood estimation we find the stream velocity at $(l, b) = (250^\circ, 50^\circ)$ from nine stars to be $V_{GSR} = 85.3 \pm 4.4 \text{ km s}^{-1}$ and the dispersion to be $6.5 \pm 7.0 \text{ km s}^{-1}$. If we exclude three stars with low signal-to-noise – and hence large ($> 10 \text{ km s}^{-1}$) velocity uncertainties – the peak occurs at $82.1 \pm 1.4 \text{ km s}^{-1}$ and the intrinsic dispersion is found to be $0.2 \pm 3.1 \text{ km s}^{-1}$. Hence, the observed stream dispersion is dominated by the velocity uncertainties, indicating that the intrinsic dispersion is small.

The K-giants presented here can provide great insight into the chemistry and history of the Orphan Stream. High-resolution spectroscopic observations have been taken for some of our highly probable members and a detailed chemical analysis will be presented in a forthcoming paper (Casey et al., in preparation). Detailed chemical abundances can help determine both the nature of the progenitor before it is discovered, and allows us to compare peculiar chemical signatures with those of the known Milky Way satellites in order to associate likely parents. However, at least for the moment, the Orphan Stream remains appropriately named.

CHAPTER 4

Conclusions

Although the Universe is under no obligation to make sense,
students in pursuit of the Ph.D. are.

– Robert P. Kirshner¹

Lorem ipsum dolor sit amet, consectetur adipiscing elit. Duis posuere tellus eu quam pellentesque ut varius purus egestas. Nam hendrerit malesuada sapien, non molestie risus cursus at. Pellentesque habitant morbi tristique senectus et netus et malesuada fames ac turpis egestas. Sed dignissim sodales sem sed volutpat. Ut laoreet, ante sed dictum vestibulum, lacus sapien semper dui, nec rutrum velit justo eu enim. Fusce vehicula blandit ipsum, ac volutpat libero vestibulum in. Sed quis lacus mauris. Quisque congue elit in nisi lacinia ac condimentum eros pellentesque. Quisque et nisl odio, vitae eleifend neque. In volutpat sapien non leo egestas ut sodales elit malesuada. Proin suscipit, lacus a suscipit euismod, neque velit pellentesque urna, eget ullamcorper felis neque sit amet erat. Phasellus in est et ligula accumsan lacinia sit amet et nisl. Aliquam interdum, arcu sed dictum gravida, mi justo iaculis mi, vel scelerisque nulla nunc in justo (?).

Phasellus erat libero, lobortis vitae iaculis nec, congue et tortor. Donec tempus leo et nisl tincidunt porta. Nulla velit sapien, sollicitudin sit amet accumsan a, facilisis a est. Phasellus scelerisque convallis sapien, nec viverra dui tincidunt a. Nulla ligula velit, laoreet fringilla condimentum sed, euismod a est. Fusce leo sapien, rhoncus a ultricies nec, porttitor ut lectus. Sed vestibulum turpis risus, nec vestibulum diam. Morbi quis quam quis enim cursus aliquam scelerisque quis tellus. Pellentesque accumsan lectus cursus massa ultrices placerat. Nulla facilisi. Praesent fermentum erat in augue sagittis condimentum. Nullam posuere blandit urna a mollis. Cras malesuada lectus a turpis sollicitudin volutpat. Morbi semper, nisl vel mattis vehicula, sapien sapien adipiscing tortor, in accumsan tortor dolor non neque. Maecenas varius, nunc ut euismod volutpat, mauris ante faucibus magna, ac eleifend elit tortor sed arcu.

¹*Quarterly Journal of the Royal Astronomical Society*. 1991, Vol. 32, No. 3, p233

4.1. Future prospects

 Lorem ipsum dolor sit amet, consectetur adipiscing elit. Duis posuere tellus eu quam pellentesque ut varius purus egestas. Nam hendrerit malesuada sapien, non molestie risus cursus at. Pellentesque habitant morbi tristique senectus et netus et malesuada fames ac turpis egestas. Sed dignissim sodales sem sed volutpat.

4.1.1. What you were going to do in your Ph.D.

 Ut laoreet, ante sed dictum vestibulum, lacus sapien semper dui, nec rutrum velit justo eu enim. Fusce vehicula blandit ipsum, ac volutpat libero vestibulum in. Sed quis lacus mauris. Quisque congue elit in nisi lacinia ac condimentum eros pellentesque. Quisque et nisl odio, vitae eleifend neque. In volutpat sapien non leo egestas ut sodales elit malesuada. Proin suscipit, lacus a suscipit euismod, neque velit pellentesque urna, eget ullamcorper felis neque sit amet erat. Phasellus in est et ligula accumsan lacinia sit amet et nisl. Aliquam interdum, arcu sed dictum gravida, mi justo iaculis mi, vel scelerisque nulla nunc in justo.

 Phasellus erat libero, lobortis vitae iaculis nec, congue et tortor. Donec tempus leo et nisl tincidunt porta. Nulla velit sapien, sollicitudin sit amet accumsan a, facilisis a est. Phasellus scelerisque convallis sapien, nec viverra dui tincidunt a. Nulla ligula velit, laoreet fringilla condimentum sed, euismod a est. Fusce leo sapien, rhoncus a ultricies nec, porttitor ut lectus. Sed vestibulum turpis risus, nec vestibulum diam. Morbi quis quam quis enim cursus aliquam scelerisque quis tellus. Pellentesque accumsan lectus cursus massa ultrices placerat. Nulla facilisi. Praesent fermentum erat in augue sagittis condimentum. Nullam posuere blandit urna a mollis. Cras malesuada lectus a turpis sollicitudin volutpat. Morbi semper, nisl vel mattis vehicula, sapien sapien adipiscing tortor, in accumsan tortor dolor non neque. Maecenas varius, nunc ut euismod volutpat, mauris ante faucibus magna, ac eleifend elit tortor sed arcu.

4.1.2. Save some work for your first post-doc

 Vestibulum sed orci nec diam euismod vehicula vitae et mauris. Phasellus sagittis justo quis mauris adipiscing auctor. Suspendisse nibh erat, cursus vitae aliquam in, rutrum sed est. Nunc mollis quam quis velit vehicula fringilla. Quisque convallis, neque ut faucibus luctus, nisl ante porttitor ante, at venenatis lectus nulla sed augue. Quisque lacinia semper lacus, nec ultricies justo auctor vel. Aenean viverra aliquam est ac porttitor.

 Aliquam egestas elementum enim, id porta libero sodales ac. Fusce mattis ultrices tortor, eget iaculis nibh ultrices et. Fusce eget ligula quam. Vivamus id nisi non sapien venenatis adipiscing. Mauris posuere imperdiet elit, vitae accumsan nibh vehicula eget. Curabitur et magna mi, vel elementum velit. Class aptent taciti sociosqu ad litora torquent per conubia nostra, per inceptos himenaeos. Donec placerat arcu eget eros ornare viverra.

Bibliography

- Armandroff, T. E., & Da Costa, G. S. 1991, AJ, 101, 1329 ([ADS entry](#))
- Battaglia, G., Irwin, M., Tolstoy, E., Hill, V., Helmi, A., Letarte, B., & Jablonka, P. 2008, MNRAS, 383, 183 ([ADS entry](#))
- Bell, E. F., et al. 2008, ApJ, 680, 295 ([ADS entry](#))
- Bellazzini, M., Correnti, M., Ferraro, F. R., Monaco, L., & Montegriffo, P. 2006, A&A, 446, L1 ([ADS entry](#))
- Belokurov, V., et al. 2006, ApJ, 642, L137 ([ADS entry](#))
- Bonifacio, P., Sbordone, L., Marconi, G., Pasquini, L., & Hill, V. 2004, A&A, 414, 503 ([ADS entry](#))
- Cacciari, C., Bellazzini, M., & Colucci, S. 2002, in IAU Symposium, Vol. 207, Extragalactic Star Clusters, ed. D. P. Geisler, E. K. Grebel, & D. Minniti, 168 ([ADS entry](#))
- Carollo, D., et al. 2007, Nature, 450, 1020 ([ADS entry](#))
- . 2010, ApJ, 712, 692 ([ADS entry](#))
- Casetti-Dinescu, D. I., Girard, T. M., Majewski, S. R., Vivas, A. K., Wilhelm, R., Carlin, J. L., Beers, T. C., & van Altena, W. F. 2009, ApJ, 701, L29 ([ADS entry](#))
- Castelli, F., & Kurucz, R. L. 2004, ArXiv Astrophysics e-prints 0405087 ([ADS entry](#))
- Chou, M., et al. 2007, ApJ, 670, 346 ([ADS entry](#))
- Deutsch, E. W. 1994, PASP, 106, 1134 ([ADS entry](#))
- Dotter, A., Chaboyer, B., Jevremović, D., Kostov, V., Baron, E., & Ferguson, J. W. 2008, ApJS, 178, 89 ([ADS entry](#))
- Downes, R. A., et al. 2004, AJ, 127, 2838 ([ADS entry](#))
- Duffau, S., Zinn, R., Vivas, A. K., Carraro, G., Méndez, R. A., Winnick, R., & Gallart, C. 2006, ApJ, 636, L97 ([ADS entry](#))

- Fellhauer, M., et al. 2006, ApJ, 651, 167 ([ADS entry](#))
- Fitzpatrick, E. L. 1999, PASP, 111, 63 ([ADS entry](#))
- Girardi, L., Grebel, E. K., Odenkirchen, M., & Chiosi, C. 2004, A&A, 422, 205 ([ADS entry](#))
- Goswami, A., Karinkuzhi, D., & Shantikumar, N. S. 2010, MNRAS, 402, 1111 ([ADS entry](#))
- Green, P. J., Margon, B., Anderson, S. F., & Cook, K. H. 1994, ApJ, 434, 319 ([ADS entry](#))
- Green, P. J., Margon, B., Anderson, S. F., & MacConnell, D. J. 1992, ApJ, 400, 659 ([ADS entry](#))
- Harris, W. E. 1996, AJ, 112, 1487 ([ADS entry](#))
- Helmi, A. 2004, ApJ, 610, L97 ([ADS entry](#))
- . 2008, A&A Rev., 15, 145 ([ADS entry](#))
- Helmi, A., & White, S. D. M. 1999, MNRAS, 307, 495 ([ADS entry](#))
- . 2001, MNRAS, 323, 529 ([ADS entry](#))
- Hinkle, K., Wallace, L., Livingston, W., Ayres, T., Harmer, D., & Valenti, J. 2003, in The Future of Cool-Star Astrophysics: 12th Cambridge Workshop on Cool Stars, Stellar Systems, and the Sun, ed. A. Brown, G. M. Harper, & T. R. Ayres, Vol. 12, 851–856 ([ADS entry](#))
- Ibata, R., Lewis, G. F., Irwin, M., Totten, E., & Quinn, T. 2001, ApJ, 551, 294 ([ADS entry](#))
- Ibata, R. A., Gilmore, G., & Irwin, M. J. 1994, Nature, 370, 194 ([ADS entry](#))
- Ibata, R. A., & Lewis, G. F. 1998, ApJ, 500, 575 ([ADS entry](#))
- Ivezić, Ž., et al. 2000, AJ, 120, 963 ([ADS entry](#))
- Jester, S., et al. 2005, AJ, 130, 873 ([ADS entry](#))
- Johnston, K. V., Law, D. R., & Majewski, S. R. 2005, ApJ, 619, 800 ([ADS entry](#))
- Jurić, M., et al. 2008, ApJ, 673, 864 ([ADS entry](#))
- Keller, S. C. 2010, Publications of the Astronomical Society of Australia, 27, 45 ([ADS entry](#))
- Keller, S. C., Murphy, S., Prior, S., Da Costa, G., & Schmidt, B. 2008, ApJ, 678, 851 ([ADS entry](#))
- Keller, S. C., Yong, D., & Da Costa, G. S. 2010, ApJ, 720, 940 ([ADS entry](#))
- Kerr, F. J., & Lynden-Bell, D. 1986, MNRAS, 221, 1023 ([ADS entry](#))
- Kurucz, R. L., & Bell, B. 1995, Atomic Line Data, Kurucz CD-ROM No. 23, (Smithsonian Astrophysical Observatory, Cambridge, MA)
- Law, D. R., Johnston, K. V., & Majewski, S. R. 2005, ApJ, 619, 807 ([ADS entry](#))
- Law, D. R., & Majewski, S. R. 2010, ApJ, 714, 229 ([ADS entry](#))
- Law, D. R., Majewski, S. R., & Johnston, K. V. 2009, ApJ, 703, L67 ([ADS entry](#))

- Majewski, S. R., Siegel, M. H., Kunkel, W. E., Reid, I. N., Johnston, K. V., Thompson, I. B., Landolt, A. U., & Palma, C. 1999, AJ, 118, 1709 ([ADS entry](#))
- Majewski, S. R., Skrutskie, M. F., Weinberg, M. D., & Ostheimer, J. C. 2003, ApJ, 599, 1082 ([ADS entry](#))
- Martínez-Delgado, D., Gómez-Flechoso, M. Á., Aparicio, A., & Carrera, R. 2004, ApJ, 601, 242 ([ADS entry](#))
- Mihalas, D., & Binney, J. 1981, Science, 214, 829 ([ADS entry](#))
- Monaco, L., Bellazzini, M., Bonifacio, P., Ferraro, F. R., Marconi, G., Pancino, E., Sbordone, L., & Zaggia, S. 2005, A&A, 441, 141 ([ADS entry](#))
- Newberg, H. J., Yanny, B., Cole, N., Beers, T. C., Re Fiorentin, P., Schneider, D. P., & Wilhelm, R. 2007, ApJ, 668, 221 ([ADS entry](#))
- Newberg, H. J., et al. 2002, ApJ, 569, 245 ([ADS entry](#))
- . 2003, ApJ, 596, L191 ([ADS entry](#))
- Prior, S. L., Da Costa, G. S., & Keller, S. C. 2009a, ApJ, 704, 1327 ([ADS entry](#))
- Prior, S. L., Da Costa, G. S., Keller, S. C., & Murphy, S. J. 2009b, ApJ, 691, 306 ([ADS entry](#))
- Roeser, S., Demleitner, M., & Schilbach, E. 2010, AJ, 139, 2440 ([ADS entry](#))
- Ruhland, C., Bell, E. F., Rix, H.-W., & Xue, X.-X. 2011, ApJ, 731, 119 ([ADS entry](#))
- Rutledge, G. A., Hesser, J. E., & Stetson, P. B. 1997, PASP, 109, 907 ([ADS entry](#))
- Ryan, S. G., & Norris, J. E. 1991, AJ, 101, 1865 ([ADS entry](#))
- Schlafly, E. F., & Finkbeiner, D. P. 2011, ApJ, 737, 103 ([ADS entry](#))
- Schlegel, D. J., Finkbeiner, D. P., & Davis, M. 1998, ApJ, 500, 525 ([ADS entry](#))
- Schönrich, R., Asplund, M., & Casagrande, L. 2011, MNRAS, 415, 3807 ([ADS entry](#))
- Siegel, M. H., et al. 2007, ApJ, 667, L57 ([ADS entry](#))
- Sirko, E., et al. 2004, AJ, 127, 899 ([ADS entry](#))
- Starkenburg, E., et al. 2009, ApJ, 698, 567 ([ADS entry](#))
- . 2010, A&A, 513, A34 ([ADS entry](#))
- Tolstoy, E., Irwin, M. J., Cole, A. A., Pasquini, L., Gilmozzi, R., & Gallagher, J. S. 2001, MNRAS, 327, 918 ([ADS entry](#))
- Totten, E. J., & Irwin, M. J. 1998, MNRAS, 294, 1 ([ADS entry](#))
- Tsujimoto, T., Miyamoto, M., & Yoshii, Y. 1998, ApJ, 492, L79 ([ADS entry](#))
- Venn, K. A., Irwin, M., Shetrone, M. D., Tout, C. A., Hill, V., & Tolstoy, E. 2004, AJ, 128, 1177 ([ADS entry](#))

Vivas, A. K., Zinn, R., & Gallart, C. 2005, AJ, 129, 189 ([ADS entry](#))

Vivas, A. K., et al. 2001, ApJ, 554, L33 ([ADS entry](#))

Watkins, L. L., et al. 2009, MNRAS, 398, 1757 ([ADS entry](#))

Xue, X.-X., et al. 2011, ApJ, 738, 79 ([ADS entry](#))

Yanny, B., et al. 2009, ApJ, 700, 1282 ([ADS entry](#))

York, D. G., et al. 2000, AJ, 120, 1579 ([ADS entry](#))

Zinn, R., Vivas, A. K., Gallart, C., & Winnick, R. 2004, in Astronomical Society of the Pacific Conference Series, Vol. 327, Satellites and Tidal Streams, ed. F. Prada, D. Martinez Delgado, & T. J. Mahoney, 92 ([ADS entry](#))

APPENDIX A

An image of a kitten

A kitten is a juvenile domesticated cat. A feline litter usually consists of two to five kittens. To survive, kittens need the care of their mother for the first several weeks of their life. Kittens are highly social animals and spend most of their waking hours playing and interacting with available companions. The word “*kitten*” derives from Middle English *kitoun* (ketoun, kyton etc.), which itself came from Old French *chitoun*. The young of big cats are called cubs rather than kittens. Either term may be used for the young of smaller wild felids such as ocelots, caracals, and lynx, but *kitten* is usually more common for these species.



Figure A.1 The aforementioned kitten

APPENDIX B

Lots of awful mathematics

We follow the standard derivation of ?. This differs from that used by ?, who follow ? in using Lindblad's original approach. ? derive the approximation in heliocentric coordinates in terms of the initial XYZ position and UVW velocity of the test particle. The two derivations are equivalent, as are the standard angular frequencies Ω , κ and ν .

We first assume a gravitational potential for the Galactic disk Φ that is axisymmetric around the normal to the disk. We also assume that such a potential is symmetric about the disk plane. In cylindrical (R, ϕ, z) coordinates the equations of motion for such a potential are:

$$\begin{aligned}\ddot{R} - R\dot{\phi}^2 &= -\frac{\partial\Phi}{\partial R} \\ \frac{d}{dt}(R^2\dot{\phi}) &= 0 \\ \ddot{z} &= -\frac{\partial\Phi}{\partial z}\end{aligned}\tag{B.1}$$

Noting that the second equation implies the conservation of angular momentum about the z axis; $R^2\dot{\phi} = \text{constant} = L_z$, the equations of motion can also be written

$$\ddot{R} = -\frac{\partial\Phi_{\text{eff}}}{\partial R} \quad \text{and} \quad \ddot{z} = -\frac{\partial\Phi_{\text{eff}}}{\partial z}\tag{B.2}$$

where the effective potential $\Phi_{\text{eff}}(R, z)$ is defined as

$$\Phi_{\text{eff}}(R, z) = \Phi(R, z) + \frac{L_z^2}{2R^2}\tag{B.3}$$

The effective potential has a minimum at $z = 0$ (by symmetry) and at $R = R_g$:

$$\frac{\partial\Phi_{\text{eff}}}{\partial R} = \frac{\partial\Phi}{\partial R} - \frac{L_z^2}{R^3} = 0 \quad \text{which means} \quad \left.\frac{\partial\Phi}{\partial R}\right|_{(R_g, 0)} = \frac{L_z^2}{R_g^3} = R_g\dot{\phi}^2\tag{B.4}$$

The *guiding centre radius* R_g therefore corresponds to a circular orbit with constant angular speed $\dot{\phi} = \Omega_g = \sqrt{(1/R)\partial\Phi/\partial R} = L_z/R_g^2$. We can approximate the effective potential around $(R, z) = (R_g, 0)$ by the second-order Taylor expansion around this point. If we define $x = (R - R_g)$ the expansion is:

$$\begin{aligned}\Phi_{\text{eff}} \simeq \Phi_{\text{eff}}(R_g, 0) &+ x\left.\frac{\partial\Phi_{\text{eff}}}{\partial R}\right|_{(R_g, 0)} + z\left.\frac{\partial\Phi_{\text{eff}}}{\partial z}\right|_{(R_g, 0)} \\ &+ \frac{1}{2}x^2\left.\frac{\partial^2\Phi_{\text{eff}}}{\partial R^2}\right|_{(R_g, 0)} + \frac{1}{2}z^2\left.\frac{\partial^2\Phi_{\text{eff}}}{\partial z^2}\right|_{(R_g, 0)} + xz\left.\frac{\partial^2\Phi_{\text{eff}}}{\partial R\partial z}\right|_{(R_g, 0)}\end{aligned}\tag{B.5}$$

The second and third terms are zero at the point $(R_g, 0)$. The cross-term is also zero as we assume the potential is symmetric about $z = 0$. The effective potential then becomes

$$\begin{aligned}\Phi_{\text{eff}} &\simeq \Phi_{\text{eff}}(R_g, 0) + \frac{1}{2}x^2 \frac{\partial^2 \Phi_{\text{eff}}}{\partial R^2} \Big|_{(R_g, 0)} + \frac{1}{2}z^2 \frac{\partial^2 \Phi_{\text{eff}}}{\partial z^2} \Big|_{(R_g, 0)} \\ &= \Phi_{\text{eff}}(R_g, 0) + \frac{1}{2}(\kappa x)^2 + \frac{1}{2}(\nu z)^2\end{aligned}\quad (\text{B.6})$$

where we define the constants:

$$\kappa^2 = \frac{\partial^2 \Phi_{\text{eff}}}{\partial R^2} \Big|_{(R_g, 0)} \quad \text{and} \quad \nu^2 = \frac{\partial^2 \Phi_{\text{eff}}}{\partial z^2} \Big|_{(R_g, 0)} \quad (\text{B.7})$$

In this second-order Taylor expansion of the effective potential the equations of motion (Eqn. B.2) simplify to those of harmonic oscillators:

$$\ddot{x} = -\kappa^2 x \quad \text{and} \quad \ddot{z} = -\nu^2 z \quad (\text{B.8})$$

which have the general solutions:

$$x(t) = X \cos(\kappa t + \alpha) \quad \text{and} \quad z(t) = Z \cos(\nu t + \beta) \quad (\text{B.9})$$

for constants X, Z, α and β . What about the azimuthal coordinate ϕ ? Realising that angular momentum is conserved and $\dot{\phi} = L_z/R^2$ and $\Omega_g = L_z/R_g^2$, we have

$$\dot{\phi} = \frac{L_z}{R_g^2} \frac{1}{(x/R_g + 1)^2} \simeq \Omega_g \left(1 - 2 \frac{x}{R_g}\right) \quad (\text{B.10})$$

Substituting for $x(t)$ and integrating we arrive at

$$\phi = \Omega_g t - 2 \frac{\Omega_g}{R_g \kappa} X \sin(\kappa t + \alpha) + \phi_0 \quad (\text{B.11})$$

If we convert the cylindrical (R, ϕ, z) coordinate system to a Cartesian system (x, y, z) , co-moving with the guiding centre (R_g, ϕ) ; for $X \ll R_g$ this simplifies to:

$$\begin{aligned}y(t) &= -2 \frac{\Omega_g}{\kappa} X \sin(\kappa t + \alpha) \\ &= -Y \sin(\kappa t + \alpha)\end{aligned}\quad (\text{B.12})$$

In the new coordinate system x and z are the same as above and y points in the direction of Galactic rotation. In this frame the star can be thought of as simultaneously oscillating around the guiding centre vertically and in an ellipse in the xy plane (the epicycle). The motion can be described by three angular frequencies; the epicyclic frequency κ , the vertical frequency ν and the angular velocity of the guiding centre, Ω_g . The vertical motion is independent of the epicyclic motion. The size of the epicycle is dictated by the ratio of κ to Ω_g : $X/Y = \kappa/2\Omega_g$. The resultant orbital motion following Equations B.9 and B.12 in a Galactocentric inertial frame is traced in Figure B.1. Like in the general case, although close to circular, the orbit is not closed in such a frame.

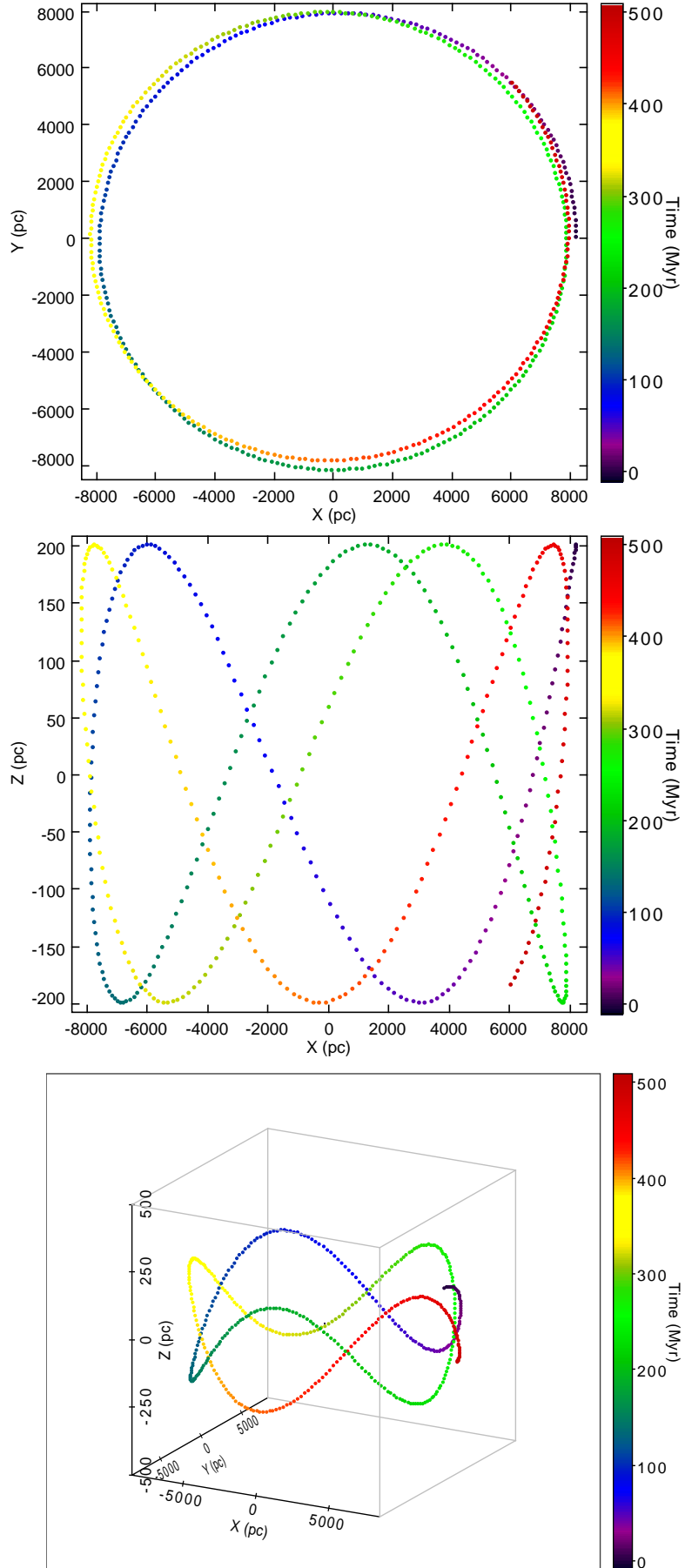


Figure B.1 Orbital motion with $\kappa_0 = 0.0367 \text{ km s}^{-1} \text{ pc}^{-1}$, $\Omega_0 = 0.0272 \text{ km s}^{-1} \text{ pc}^{-1}$, $R_g = R_\odot = 8000 \text{ pc}$ and $X = Z = 200 \text{ pc}$. The coordinate system has its origin at the Galactic centre.